2011

Development of Measurement Methods for Testing of Hydrokinetic Devices to Evaluate the Environmental Effect on Local Substrate

Michael Volpe
Bucknell University

Development of Measurement Methods for Testing of Hydrokinetic Devices to Evaluate the Environmental Effect on Local Substrate

by

Michael A. Volpe
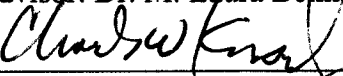
A Thesis Submitted to the Honors Council

For Honors in Mechanical Engineering

May 2011

Approved by:

Advisor: Dr. M. Laura Beninati, Mechanical Engineering Department

Department Chairperson Dr. Charles Knisely, Mechanical Engineering Department

Table of Contents:

Table of Figures:

Abstract

Modifications and upgrades to the hydraulic flume facility in the Environmental Fluid Mechanics and Hydraulics Laboratory (EFM&H) at Bucknell University are described. These changes enable small-scale testing of model marine hydrokinetic (MHK) devices. The design of the experimental platform provides a controlled environment for testing of model MHK devices to determine their effect on local substrate. Specifically, the effects being studied are scour and erosion around a cylindrical support structure and deposition of sediment downstream from the device.

In order to assess the impact of deploying large arrays of MHK devices in rivers and tidal estuaries, experiments must be performed at the early stages of these studies. Small-scale studies are a cost-effective means to predict possible environmental effects on a larger scale. This data is also crucial to validate numerical computations used in designing of these devices to minimize their deleterious impact on the environment. This testing platform for laboratory-scaled studies is instrumental in yielding physical measurements of MHK wake-induced changes to the sediment. These results will help predict how these devices behave in real world environments.

An insert has been designed to hold sediment of desired size and material to allow for a multitude of environments to be tested. Downstream of the test section is a set of collection bins to catch displaced sediment to control its dispersion within the facility. The test bed is of sufficient size to accommodate either a single model MHK device or an array of devices to evaluate potential arrangements in river environments. A nozzle insert has also been designed to increase the range of flow speeds available for

model device testing. The device accelerates the flow through the nozzle by decreasing the cross-sectional area by a factor of two. The flume facility also has a programmable 3D traversing system that can accurately place an Acoustic Doppler Velocimeter (ADV) probe anywhere along the length, width and depth of the flume to within +/- 0.001 inches. Using ADV characterization of flow in the nozzle sediment insert, both span-wise velocity profiles and boundary layer profiles are evaluated within the test section. The facility is also equipped with a 2D sediment bed profiler consisting of both a low-powered laser probe and a touch sensitive probe that accurately measure the topology of the sediment bed. The laser probe can be used in both air and water and works by maintaining a constant distance between the laser sensor and the bed. All of the instruments being used in the facility are non-evasive to the measurements being taken.

A full flume velocity profile both with and without the nozzle insert was created using the ADV by measuring velocities at various points in the flume. Furthermore, measurement methods were created to calculate the amount of displaced sediment using a 2D sediment bed profiler. Finally, a sluice gate and straightener were added to the flume to help condition the flow. Velocity measurements and energy calculations were used to validate the use of these devices so baseline reference conditions could be evaluated for future testing using the experimental platform.

1. Introduction

1.1 Background

1.1.1 Marine Renewable Energy

Marine renewable energy is a growing possibility as a way to harness power to provide electricity to residential and commercial districts. Energy is extracted from oceans and other tidal waterways that provide strong currents, similar to wind energy, used to push turbine blades connected to a shaft. The two main sources of marine energy are wave energy and hydrokinetic energy. Wave energy is harnessed by floating a bob at sea level, with connections to structures anchored on the sea floor. The change in height of the waves displaces the bob, thus creating motion in the structures below which takes energy away from the wave. Hydrokinetic energy is harnessed using the force of water across a set of turbine blades which causes it to rotate and produce energy. This type of energy system will most likely be found in rivers and other tidal waterways. Currently in the United States, conventional hydropower is the main type of water power. Hydropower plants convert potential energy from a reservoir created by the placement of dams to produce electricity. The water is stored behind the dam as potential energy through a large hydrostatic pressure head then fed to large hydraulic turbines which spin and convert energy to shaft work which then powers a generator. The idea behind hydrokinetic energy is to use the kinetic energy of the flow in a river or tides in an estuary to rotate the blades of a device, thus converting it to electrical power. In common terms, hydrokinetic power is taking a wind farm and putting it underwater. The drive to extract marine energy has been motivated and supported by government grants channeled down from national research laboratories to colleges and universities.

1.1.2 Governmental Support/Motivation

The Committee on Science and Technology in the U.S. House of Representatives has pushed for the initiative to discover and utilize new sources of renewable energy. The Marine Renewable Energy Research and Development Act of 2007 (H.R. 2313) "directs the Secretary of Energy to support programs of research, development, demonstration, and commercial application in marine renewable energy technologies. It also [seeks to] establish National Centers for the testing of marine renewable energy technologies" (Marine Renewable Act 2007). The bill has appropriated $50,000,000 a year from 2008 – 2012 for further development of marine renewable energy technologies. The Bucknell University hydraulic flume facility is hosting a project funded by Sandia National Laboratories through the Department of Energy to aid in the scientific research necessary (specifically the environmental effect on local substrate) for the addition of marine hydrokinetic power as a viable source of renewable energy in the United States. Some of these environmental effects for the different types of marine renewable energy devices can be seen in Figure 1.
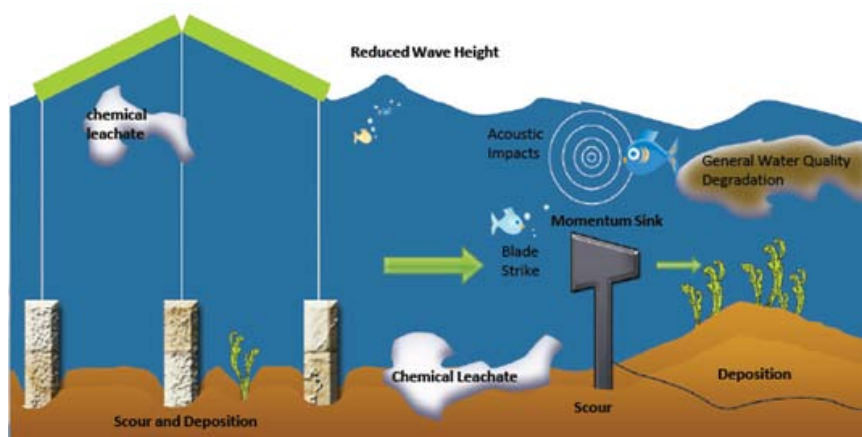
Figure 1: Possible environmental effects on substrate (adapted from Sandia National Laboratories).

For *wave energy*, the existence of the support structures for the bob anchored at the sea floor will cause scour and deposition of the surrounding bed. The extraction of energy from the waves will cause reduced wave height and may impact the normal flow of the ocean. Deterioration of the devices may also cause the presence of a chemical leachate which may harm the surrounding marine life. For *hydrokinetic power*, the spinning blades may strike fish and the extraction of energy may cause a momentum sink behind the structure. The erosion around the support structure at the base of the device may cause scour and disrupt the habitat of creatures in the substrate. Also, the deposition on the sea floor will cause large sediment piles downstream of the device. In some of the early developments of marine renewable energy technologies, the United Kingdom and the United States have come across challenges and setbacks in their progress in developing these technologies.

1.1.3 Marine Current Turbines Ltd (UK)

In the United Kingdom (UK), Marine Current Turbines Ltd launched a project to design a commercial tidal energy power plant based on the concepts used for wind energy extraction. The company currently has a working tidal mill located in the English Channel off the coast of Devon, England. The tidal mill is cemented into the bed of the channel approximately 1.1 km off the coast. The tidal mill rig rises a few meters above the water's surface. The rotor configuration is 11 meters in diameter and is capable of reversing direction to compensate for the change in flow direction with changing tides (Lang 2003). A digitally created image of the tidal mill is shown in Figure 2.
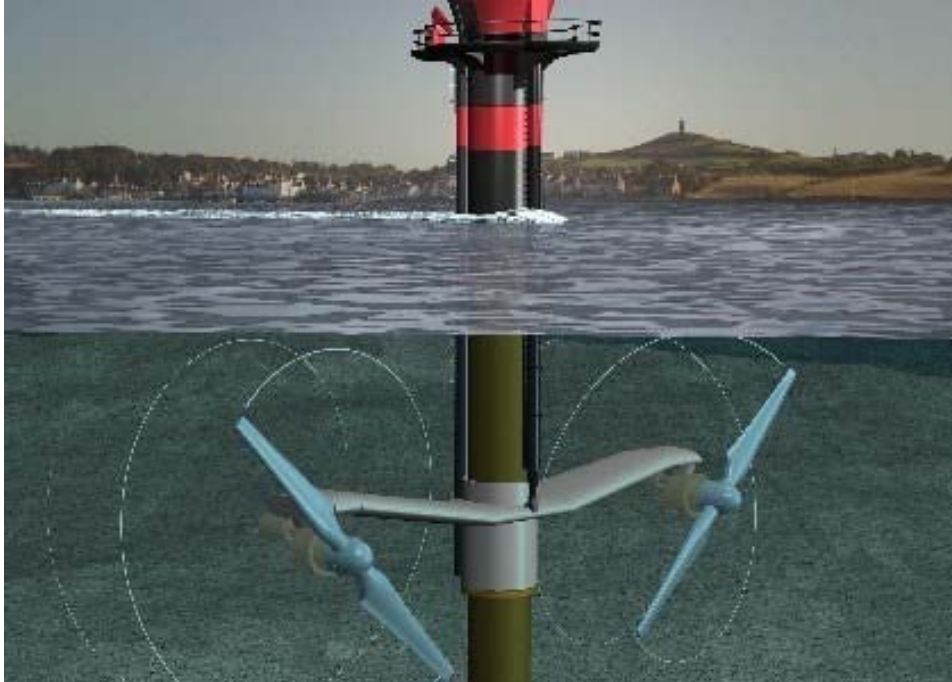
Figure 2: Marine Current Turbines Ltd device (taken from http://www.marineturbines.com/).

Compared to wind turbines, the blades underneath the water rotate slowly, (i.e. 17 RPM) as water is approximately 800 times as dense as air. With appropriate gearing, the tidal mill harnesses sufficient tidal energy to drive the large blades to rotate the generator with frequency appropriate for power generation. On average, the tidal mill is capable of producing 100 kW with peak power generation of 300 kW. To produce adequate power, it must be placed between 66 – 98 feet deep and the minimum speed of the tidal currents must be 7.4 – 8.2 feet per second (Lang 2003). Similar to the United Kingdom, Verdant Power in the United States is making progress in the installation of renewable energy devices.

1.1.4 Verdant Power (US)

In the United States, Verdant Power is currently taking steps toward introducing hydrokinetic energy to the power grid through an array of tidal turbines placed in the East River in New York called the Roosevelt Island Tidal Energy (RITE) project which was initiated in 2002. As design failures in the East River project persist, further design and testing is crucial to the success of harnessing hydrokinetic power. Verdant Power deployed six turbines in the river in December 2006 that "were capable of supplying 1,000 daily kilowatt hours of power" (Hogarty 2007). A picture of the turbines as they sit on a barge on the river is shown in Figure 3.
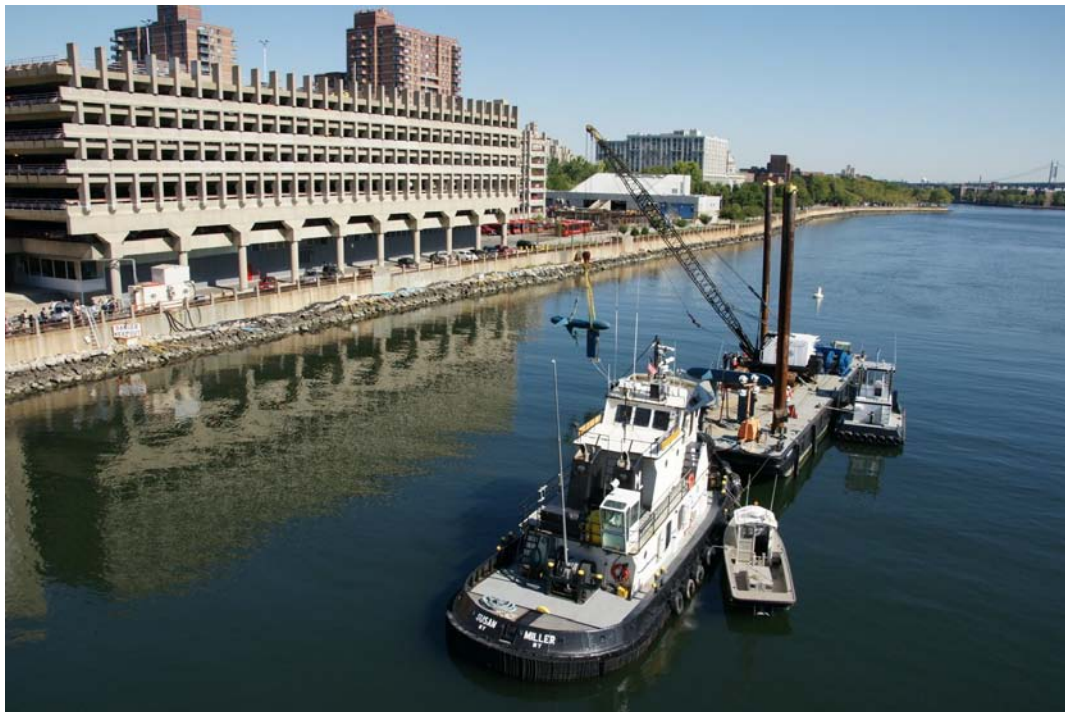
Figure 3: Verdant Power's RITE Project (taken from http://verdantpower.com/what-initiative/).

Due to the strong currents in the East River, the company removed turbines out of the water with "[blades] that were sheared off a third of the way down" the length of the

blade, caused by cavitation erosion (Hogarty 2007). Cavitation is the formation of gas bubbles in flowing liquid that form when the pressure of the liquid falls below its vapor pressure. Due to the changes in pressure, these bubbles collapse causing cyclic stresses on the metal surface, thus eroding the material surface of the turbine blades. Observing the struggles shown by this company alone, it is very important to have inexpensive methods for small-scale laboratory testing or extensive field testing of a prototype turbine design to accelerate the development of technology for marine hydrokinetic energy extraction. Additionally, the devices were not in the water long enough for all of the environmental effects (i.e. aquatic life, substrate, fouling) to be observed and documented to assess the total impact on the surroundings.

1.2 Significance

In order to preserve the environment and the habitation of the rivers and tidal estuaries that will be used for power generation, studies must be done on a small-scale in a laboratory setting to be able to predict possible environmental effects on a larger scale. This data is crucial to know in advance to aid in the validation of numerical computations for the eventual implementation of these devices to have a minimal environmental footprint. The challenge of this thesis project lies in the fact that for MHK devices a system of standards on how to construct a proper scaled-down testing facility are not readily available. Also, measurement methods must be built upon available information from other areas of study. The addition of the induced swirl from the rotating MHK device must also be accounted for, beyond just scour and erosion from support structures. A platform with baseline conditions will enhance the validity of testing and provide much

needed knowledge on environmental effects and how they will impact decisions in the future to accelerate technology development.

2. Thesis Statement

2.1 Statement

The goal of this thesis project will center on the development of new measurement methods with a unique combination of instrumentation to create a small-scale laboratory testing platform for model hydrokinetic turbines. Once a viable methodology is attained the environmental effect of devices on the local substrate can be facilitated. Specifically, power extraction measurements, scour and erosion patterns and sediment transport can be investigated to see how actual river beds may behave through the implementation of underwater turbines. The way in which these objectives will be pursued is outlined in the four statements below.

1 – Characterize the flow velocity in the hydraulic flume facility and develop methodology for repeatable velocity field measurements using the Acoustic Doppler Velocimeter (ADV).

2 – Develop a flow device to increase the velocity in the flume for appropriate power extraction experiments.

3 – Develop methods to determine how much sediment is displaced (through scour and erosion) by the presence of model devices through use of a two-dimensional bed profiler which yields bed form topology.

4 – Define baseline reference conditions of the hydraulic flume facility with appropriate flow control devices as a function of flow rate to be used as a comparison for parametric studies conducted in the future.

3. Equipment

3.1 Facility

In the College of Engineering at Bucknell University, the Environmental Fluid Mechanics and Hydraulics Laboratory (EFMH) contains a 32 feet long, 4 feet wide, 15 inch tall flume in the basement of Dana Engineering building. A 3D model of the flume and the closed system by which it runs can be seen in Figure 4.

Flow direction

Orifice-plate meter

Pump

4000 gallon holding tank
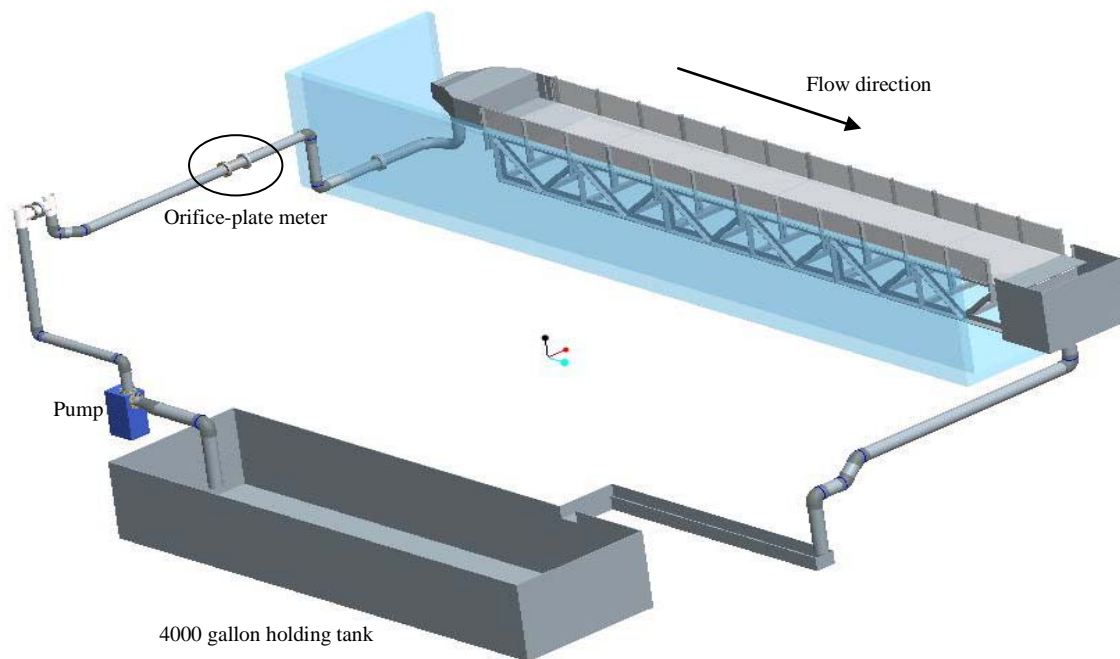
Figure 4: 3D model of hydraulic flume.

The flume facility consists of a 4000 gallon holding tank in which a 10.5 inch diameter impeller, 1780 rotations per minute (RPM), centrifugal pump made by Goulds

Pumps, Inc (Model # 3796) draws water from the tank. The water is pumped through 8-inch PVC piping into flexible tubing that dispenses the water into a diffuser and flows down the length of the flume. The water drains into a collecting device that draws through a trough and back to the holding tank. The pump, as part of the flume facility, is capable of producing a flow rate ranging from 0-1000 GPM. The flume can also be tilted from -0.27 to 1.80 degrees. The flow rate of the water is determined by an orifice meter located in the PVC piping prior to entering the diffuser. A typical orifice meter (shown in Figure 5) operates by relating the pressure and velocity of the water to determine the flow rate. An orifice meter is a thin plate with a hole located on the central axis. The fluid is forced to converge through this annular slot. Downstream of the slot a vena contracta is formed, which is the point of maximum convergence of the water where the velocity increases and the pressure decreases. The fluid pressure is measured upstream and downstream of the plate and the volumetric flow rate, $\dot{V}$, can be calculated using an energy balance where:

$$\dot{V} = C_D A_o \sqrt{\frac{2(P_1 - P_2)}{\rho(1 - \beta^4)}}, \tag{1}$$

where: C_D is the discharge coefficient,
A_0 is the cross-sectional area of the throat or orifice,
P is the pressure of the fluid,
ρ is the density of the fluid, and
β is d/D, the ratio of throat diameter to pipe diameter.

The correction factor accounting for both the frictional losses and the differences in the vena contracta area and the flow area of the obstruction is called the discharge coefficient, denoted by C_D (Cengel and Cimbala 2010). A typical value for discharge

coefficient for an orifice plate meter is 0.61 while the coefficient for a flow nozzle measuring device is 0.96. Although these are typical values, the drag coefficient also depends on the dimensions and specifications of the orifice meter as well as how it is calibrated.
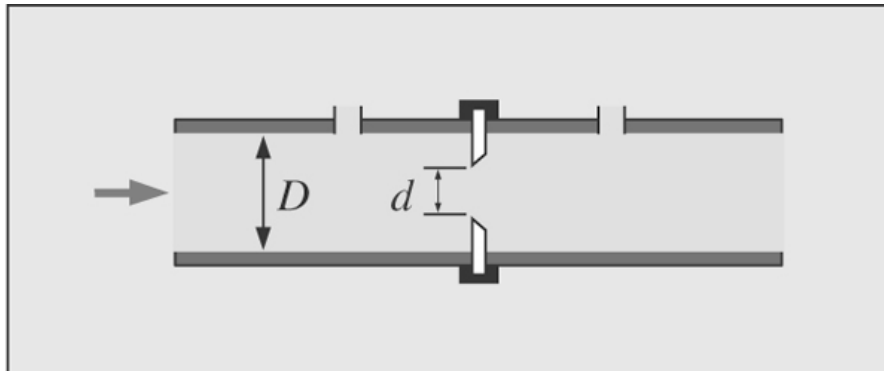
Figure 5: Orifice plate (taken from Cengel and Cimbala).

The flume is fitted with a track that spans the entire length, width and depth of the flume which allows a 3D positioning device (gantry) instrumented to accurately and repeatedly move to any point within the flume. Mounted to the gantry is a velocity measuring device and a point gauge measuring vertical displacement. Probes and other instrumentation can be interchanged on the gantry which makes it an essential tool in making repeatable measurements at any specified locations. Figure 6 shows a downstream view of the flume with the track and 3D positioning device near the end of the flume and the control panels on the left side wall. Figure 7 shows a picture of the gantry device with labeled axes of movement.
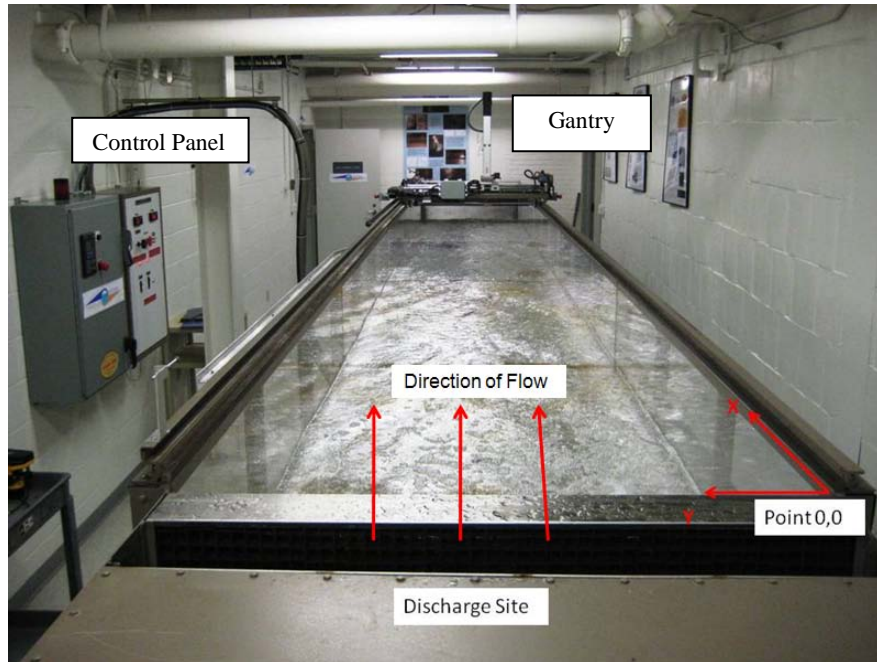
Figure 6: Downstream view of flume.
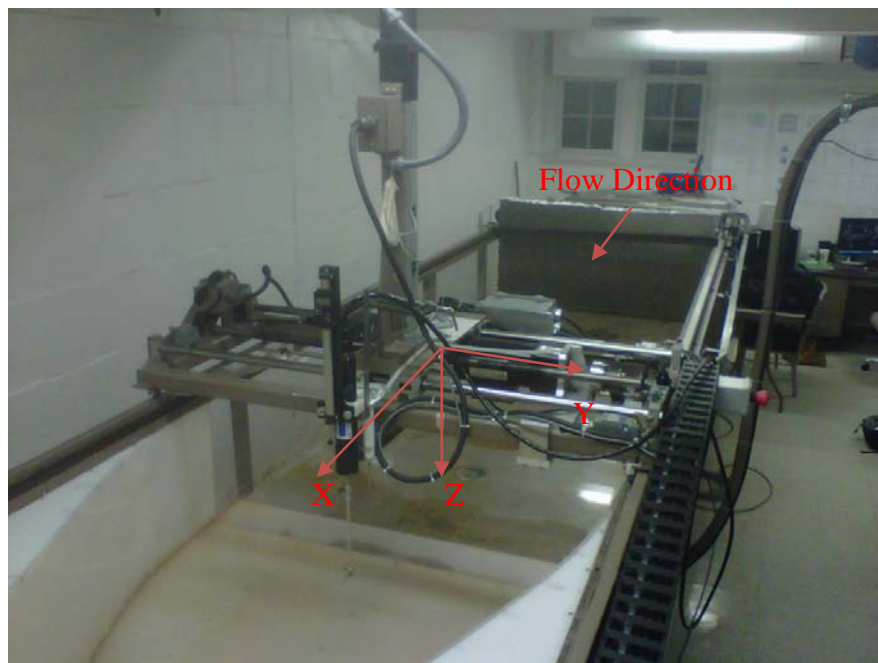
Figure 7: X, Y, and Z direction of gantry.

3.2 Measurement Devices

3.2.1 Sontek Horizon Acoustic Doppler Velocimeter (ADV) Probe

The Sontek Horizon ADV system is capable of measuring the velocity of particles using the phase change of sound wave pulse-pairs within a sampling volume using the Doppler shift theory. For a single sound wave, the velocity is obtained using the frequency shift of an emitted sound wave due to the reflection of the wave off a moving particle. The equation used to calculate the Doppler frequency of the wave is given by (Sontek Manual):

$$F_{Doppler} = -F_{source} \frac{V}{C}, \tag{2}$$

where: $F_{Doppler}$ is the change in received frequency (Doppler shift),

F_{source} is the frequency of the transmitted sounds,

V is the velocity of the particles relative to the receiver, and

C is the speed of sound in water.

A picture of the ADV probe and a model of the probe and sampling volume are shown in Figure 8 and 9, respectively.

Figure 8: Sontek ADV mounted on gantry.
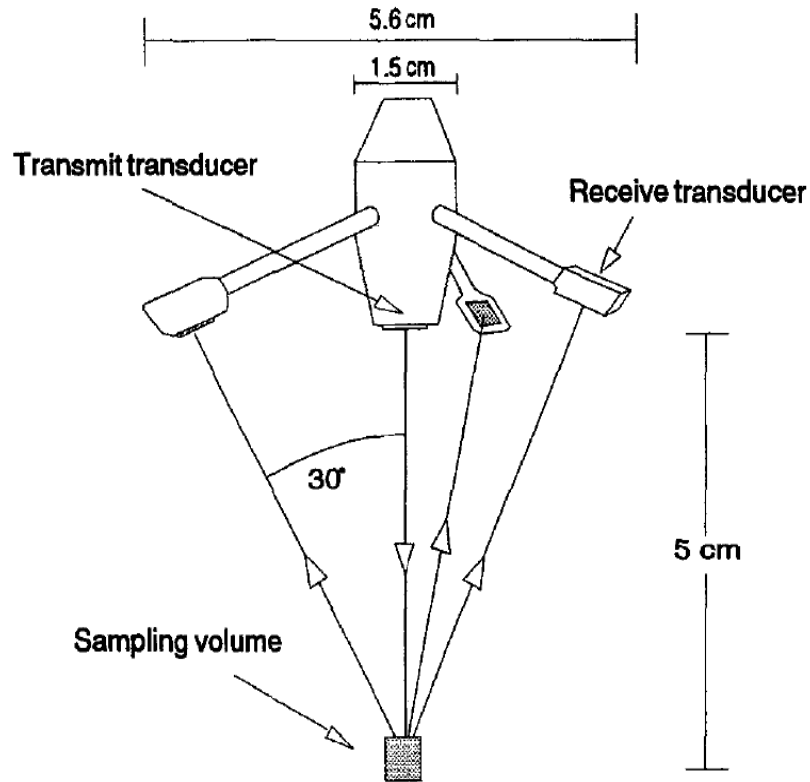
Figure 9: Drawing of ADV system (Taken from Sontek Manual).

The probe is a 16 MHz 3D MicroADV with a measurement sampling range that can vary from 0.1 – 50 Hz and a cylindrical sampling volume of 0.09 cubic centimeters. The pulse emitter is positioned a distance of 5 cm to the sampling volume with a velocity resolution of 0.01 cm/s and an accuracy of 1% of the velocity range. The ADV works on the basis that the phase shift between the received beams of the dual pulse wave is converted to a velocity. The phase shift is dependent upon the time between transmissions, phase angle and travel time. The phase angle is defined as the angle, in radians, between the shifted wave and the y-axis on the coordinate plane. The radial velocity, U, is measured using the ADV probe with the following equations (Voulgaris and Trowbridge 1998):

$$U = \frac{c\left(\frac{d\theta}{dt}\right)}{4\pi f}, \tag{3}$$

where: f is the ADV operating frequency (16 MHz),

c is the speed of sound, and

θ is the phase angle,

$$\frac{d\theta}{dt} = \frac{1}{\tau}\tan^{-1}\left[\frac{s(t)c(t+\tau)-s(t+\tau)c(t)}{c(t)c(t+\tau)+s(t)s(t+\tau)}\right], \tag{4}$$

where: s(t) and c(t) are sin(θ(t)) and cos(θ(t)), respectively, and

τ is the time between transmissions.

The probe emits two square sound waves which constitutes a pulse pair with a frequency of 16 MHz for each pulse-pair. Square sound waves are used in electronics and signal processing and are a type of non-sinusoidal waveform that alternate instantaneously between two levels. These sound waves are emitted at intervals dependent upon the sampling rate and the velocity range at which the particles are moving. The velocity range is user defined and determines the repetition rate for each pulse-pair. The repetition rate of the first pulse-pair is very small so that the ADV can compensate for the location of the phase change within one of the four quadrants. The rate of the second pulse-pair is larger to allow for more accurate velocity measurements. The ADV uses the information from the pulse-pairs to create a radial velocity. Using a transformation matrix, the radial velocity is converted to Cartesian coordinates. This data is then averaged together to form a sample (Garcia 2005).

The time, T, required to make a single measurement is given in Equation 5 (McLelland and Nicholas 2000):

$$T = 3(\tau_1 + \tau_D + \tau_2 + \tau_D),$$ (5)

where: τ_1 is the repetition rate for the first pulse-pair,

τ_2 is the repetition rate for the second pulse-pair, and

τ_D is the time between pulse-pairs (dwell time).

Once the ADV has collected all the data, it averages the x-, y-, and z-axis velocities from three receivers. The average of these values is output as a single sample. Averaging these values takes time to calculate and must be completed before the next sampling period begins.

A single sample output by the ADV is a collection of many measurements. For one sample, the ADV collects data from all 3 receivers for a set time interval controlled by the sampling rate. Higher sampling rates mean an overall shorter time period for measurement and thus less data is averaged per sample. Each measurement from the ADV requires 6 pulse-pairs: 2 for each receiver (x, y, and z). The time required for a measurement constrains the amount of measurements made per sample. A graphical representation of the pulse-pair system for a single measurement of T = 0.003792 seconds at 250 cm/s is shown in Figure 10. Table 1 shows the variation in parameters with varying velocity range presets.
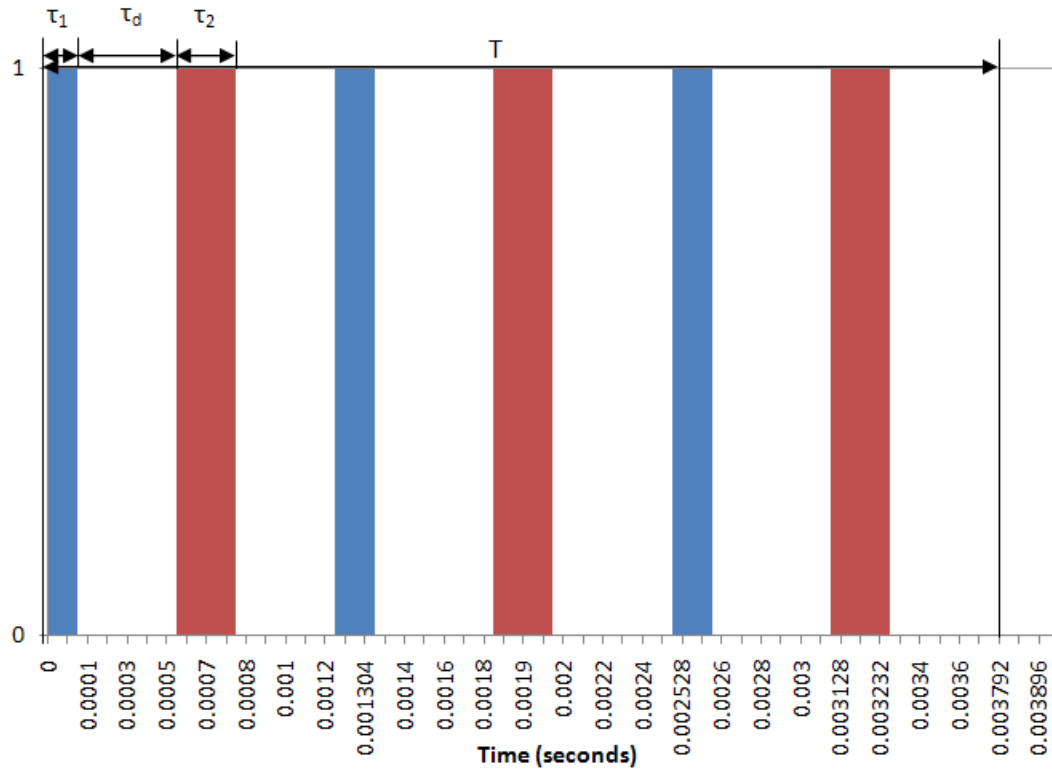
Figure 10: Chart of a single measurement at 250 cm/s (first pulse pair in blue, second in red).

Table 1: Parameters that vary with sampling rate and velocity range.

	(x 10^-6 s)			# of Measurements per Sample at Sampling Rate (Hz)						
Velocity Range (cm/s)	τ1	τ2	Velocity Measurement Time	1	5	15	25	35	45	50
250	40	104	0.003792	263	52	17	10	7	5	4
100	48	128	0.003888	256	51	16	9	7	5	4
30	112	240	0.004416	226	45	14	8	6	4	4
10	240	480	0.005520	180	36	11	7	4	3	3
3	400	800	0.006960	143	28	9	5	3	3	2

ADV Uncertainty

The velocity measurements taken by the ADV have a main source of error based on Doppler noise. The ADV user manual cites a maximum error of +/- 0.1% of the measured velocity with +/- 0.25 cm/s zero offset (Sontek Manual). As a validation that the data is accurate and usable, the manual presents two quantities to be checked during acquisition: (1) the signal to noise ratio (SNR) which is the difference between the peak sound of the received wave to the baseline noise level (Krause 1994); and, (2) the correlation coefficient which is a ratio of the coherent signal strength to the total signal strength of each received signal. One correlation is output per receiver (three in total) given by the equation (Fisher, Miller, Quick 2002):

$$Correlation = \frac{S_i{}^2}{(S_i{}^2 + N_i{}^2)},$$ (6)

where: S_i is the coherent signal strength, and

N_i is the noise in each received signal.

The Sontek manual recommends that the SNR value should be greater than 15 dB and the correlation should be above 70% for reliable measurements. Doppler broadening, velocity shear and errors due to phase ambiguity are the three main causes of the noise component in a velocity measurement. These three combine to a total variance value for a velocity measurement.

In order to place the ADV probe in the same location to take repeatable measurements, the 3D positioning device is used to move the probe to set locations in the flume.

3.2.2   3D Positioning Device

The traversing gantry, with the capability to connect various measuring probes, is moved through three stepper motors which includes feedback to the control panel with manual settings of displacements from the user-defined origin.   The system can be programmed with up to 99 presets to easily position the device in certain set locations for repeated measurements.

The gantry, shown in Figure 11, can move in the x-, y- and z-directions. Each of the three stepper motors is accurate in placing the gantry at the predetermined locations, as was determined with verification measurements to make sure the same 3D location was precisely reached. This was verified by directing the gantry to different locations, then set back to the initial position and measurements were taken manually to make sure the device reached the correct location with minimal error. The error in the gantry device in repeatedly placing the ADV in precise preset locations is approximately +/- 0.001 inches.
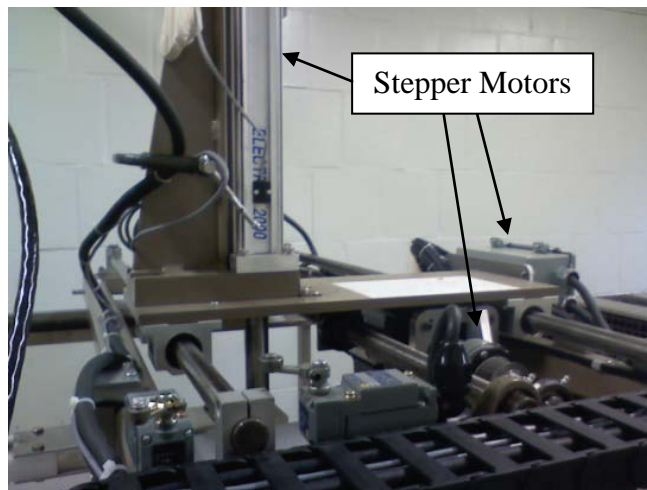
Figure 11: 3D positioning device (gantry).

Due to the limited number of available preset locations, presets can be changed and re-defined based on the experimental tests and how many total points are needed.

3.2.3 *Tailgate Flow Control Device*

At maximum flow rate, the water in the flume can only reach depths of up to 3 inches. In order to attain larger flow heights for model testing in the flume, a tailgate (or weir flow control device) was installed at the end of the flume outlet. Different tailgate heights (3", 4", 5", 9") were tested to achieve proper flow heights. The tailgate plates are bolted and unbolted onto the support structure and anchored in place with support brackets that are clamped to a cross-brace at the end of the flume as shown in Figure 12. Since the maximum diameter of the model MHK device to be tested is approximately 4 inches, it was deemed necessary to have at least one diameter of water above and below the model, yielding 12 inches of water depth in total. This helps maintain consistency and prevent any unwanted boundary or surface effects for the experimental conditions. A picture of the tailgate is shown in Figure 12. A depiction of the model turbine in place with appropriate water depth is shown in Figure 13.

Figure 12: 9 inch tailgate
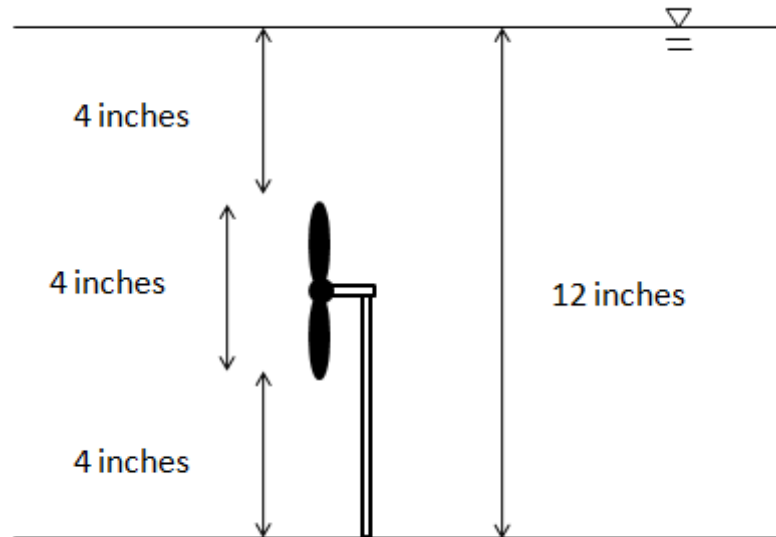
Figure 13: Model turbine with appropriate water depth.

At 800 GPM, this volumetric flow rate creates a 3 inch overflow depth (height of the water that flows above the tailgate obstruction in the flume) over a 9 inch tailgate which is used to produce a consistent depth of 12 inches throughout the flume. The flow of the water over the tailgate with a 9 inch plate is shown in Figure 14.
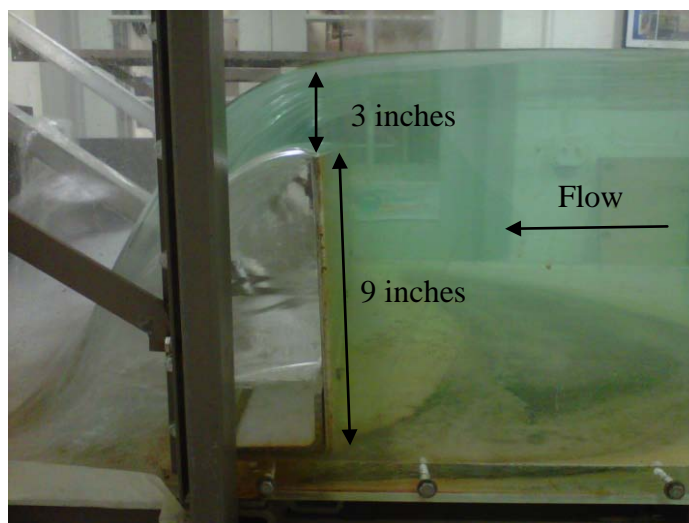
Figure 14: 9 inch tailgate with nappe.

3.2.4   Sediment Insert

The main purpose of the insert is to hold sediment in a test section for experimentation. The design for the test section is a 2 feet by 2 feet by 3 inch deep square hole. In order to create the depth, the insert has a ramp which starts flush with the bed of the flume and rises to 3 inches over a distance of approximately 55 inches. Figure 15 is a picture of the entire insert as it is located in the flume.
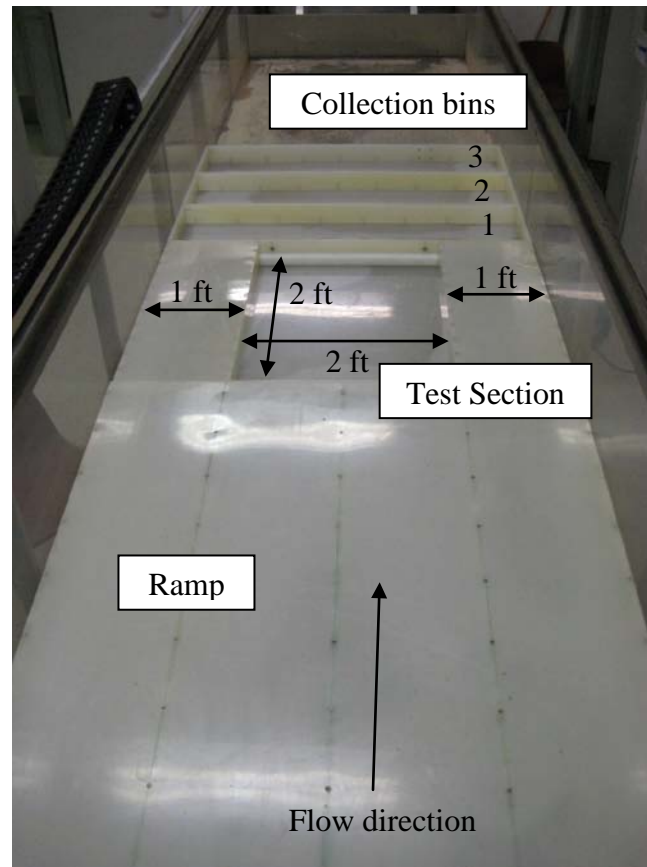
Figure 15: Overhead view of sediment insert.

Following the ramp, the test section allows for a volume of 432 cubic inches of sediment. The test section is located in the middle of the insert (12 inches in from each wall) to avoid any wall effects or boundary conditions from the sides of the flume. This

location is important because the MHK model device with sediment is tested in this area. After the test section is the collection portion of the insert which is used for retaining displaced sediment from the scour induced by the flow. There are three sections which are used to collect the sediment before being washed away downstream. The insert is approximately 10 feet long, which accounts for about a third of the total length of the flume. Pictured in Figure 16 is a cross-section of the sediment insert to illustrate the ramp, test section, and three baffles behind the test section to collect sediment.

Figure 16: Cross-section of sediment insert with sediment.

3.2.5   Significance of Components

Each component in the flume plays an important role to the success of the experimental set-up. The goal of the set-up is to replicate an environment in which model hydrokinetic devices will be placed. It is important that the overall testing platform has components that will allow for repeatable measurements, have minimal effects on the integrity of the measurements and replicate the desired environment in the best way possible. The specific purpose of each component contributes to the overall effectiveness of the platform in separate ways. The *ADV* is the instrument used to make measurements, specifically to characterize the flow by measuring velocities at given points. The *3D positioning device* is used to accurately place the probes, such as the

ADV, in locations for repeatable measurements. The *tailgate* is used to maintain the water height, one diameter above and below the model MHK device, for testing. The *sediment insert* is where sediment can be placed in the flume in a controlled manner. The test section allows for a focal point in the flume where the effects of sediment scour and erosion due to flow conditions can be isolated and measured without any boundary effects from the side walls of the flume.

4. Results and Analysis

4.1 Flow Velocity in the Hydraulic Flume Facility – Preliminary Testing

A basic understanding of the capabilities of the flume was attained and documented before any further steps were taken to modify the flume. Using the ADV, velocity profiles along the width and length of the flume were created at different flow rates and pitch angles without any components in place (i.e. sediment insert, flow control devices). Over the course of creating these profiles, a methodology for repeatable velocity measurements was developed. A literature review of the ADV system was conducted to understand how the probe works to validate its use as an accurate instrument to measure water velocity. An in-depth review of the probe was provided in Section 3.2.1 of this thesis.

A full flow velocity characterization in the flume at different locations was necessary to determine the optimal location for placement of model MHK devices to conduct experiments. Velocity samples were taken every 5 feet along the axial length of the flume. Six data points were taken at each of these downstream locations along the

transverse width of the flume. The data points were taken 0.5 feet from the origin in the transverse direction with each successive point in increments of 0.5 feet until reaching 3 feet. Figure 17 shows the locations of the data points taken for the full flume flow velocity characterization.
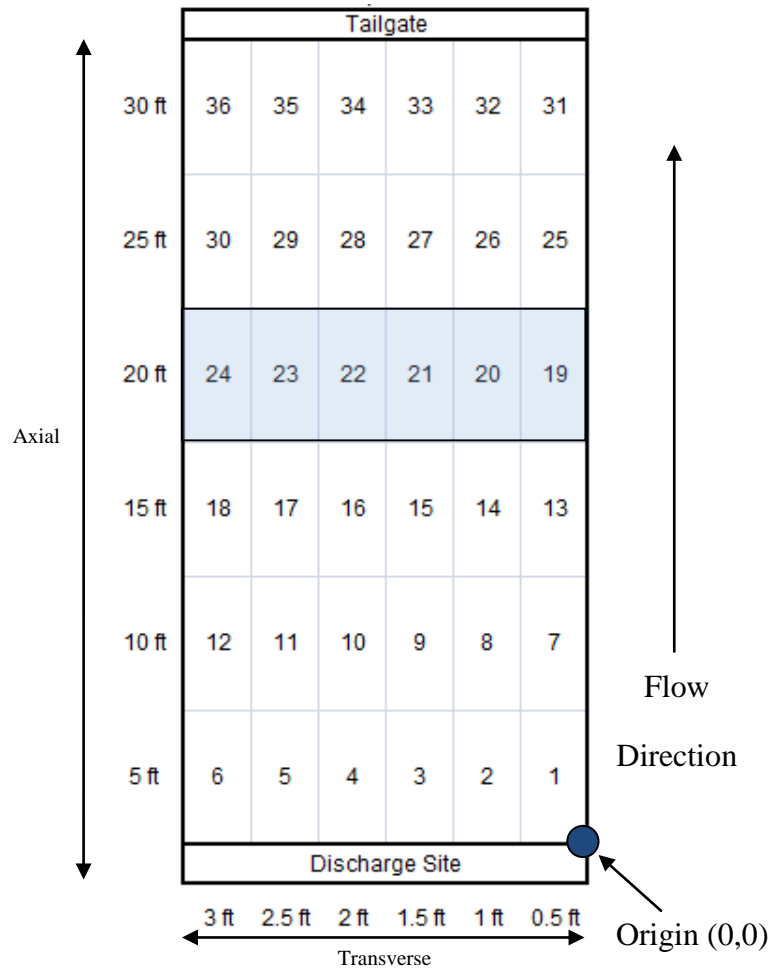
Figure 17: Overhead view of flume with test point matrix.

Each sample was measured for one minute and the data was compiled and analyzed in Microsoft Excel. All data values recorded were a measurement of the x-component of velocity in the direction of flow. The average water depth was 12 inches.

Figure 18 depicts the results of the test. Within the 6 sets of axial locations along the length of the flume, a recurring arcing trend can be observed. The average velocity for the set of all axial and transverse data locations was approximately 0.47 ft/s (average velocity throughout the entire flume). Due to: the relatively small fluctuations in the velocity profile across the 20 feet axial location; a large volume of space available both upstream and downstream (shown in Figure 17); negligible tailgate effects; and back water accumulation, this area was determined to be best for locating the testing section.
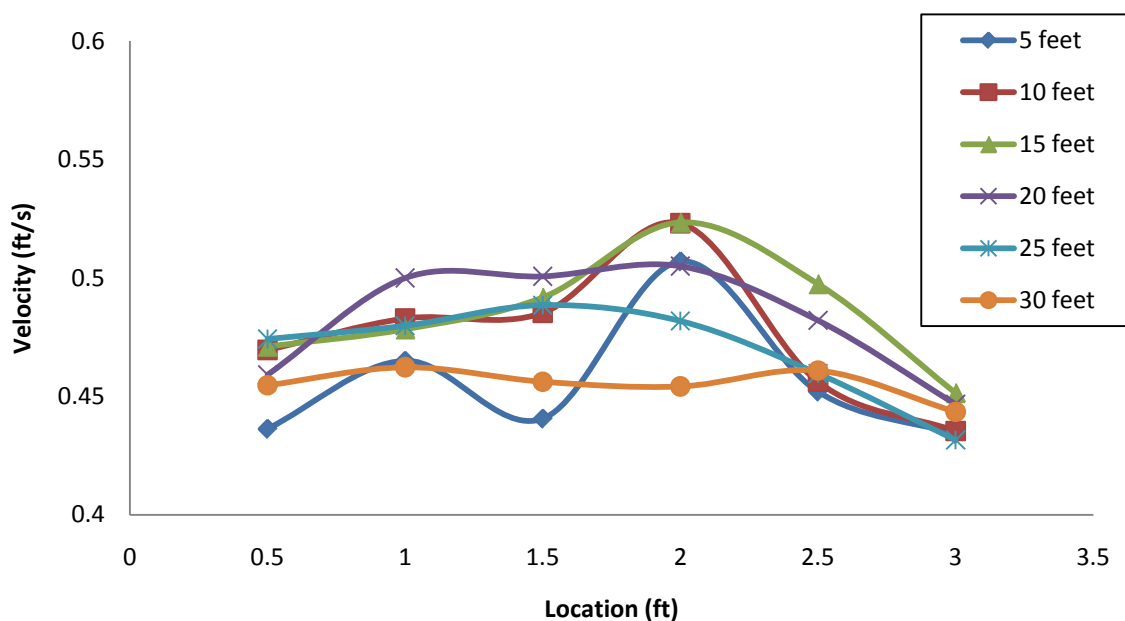
Figure 18: Full flume velocity profile (sampling volume height (z) is 6 inches from bottom of flume).

Discrepancies in the velocity profiles at the different axial locations in the flume can also be attributed to the sampling volume being maintained at the same vertical plane height while slight variations in the water height along the length of the flume were noticed. Since the velocity of the fluid is maximum at the surface of an open channel flow, the sampling volume being closer to the surface at low water depths results in

higher velocities. Although the flow velocity profiles shown in Figure 18 are not uniform, it is an improvement over the initial velocity profiles generated prior to inserting angle irons into the diffuser. This was done to help create a more even velocity profile across the width of the flume. The angle irons in the diffuser create resistance in the flow and cause a more even distribution of velocity across the width of the flume. Figure 19 shows an overhead view of the diffuser with the flow conditioning devices.

Figure 19: Flow conditioning devices in diffuser.

The next step in understanding the facility was using the tilting capabilities of the flume to demonstrate the effect on the flow velocity. Testing was done at 0.4, 1.0, and 1.4 degree slopes at one flow rate: 800 GPM. These slopes were chosen based on the facility limitations. The values span a wide range of slopes which help illustrate the behavior of the flow velocity as a function of the tilt angle. As shown in Figure 20, at 0.4

degrees, the velocity profile was fairly constant at 0.5 ft/s. At 1.0 degree, 0.5 feet from the origin in the transverse direction, the flume experienced a higher water velocity of 0.63 ft/s while 3 feet from the origin in the transverse direction the velocity was 0.48 ft/s. As the slope increased to 1.4 degrees, the velocity profile in the flume demonstrated a preferential direction at the 0.5 feet transverse location due to the presence of flow disturbances in the water inlet diffuser. The velocities ranged from highest to lowest across the flume with a difference of more than 1 ft/s.
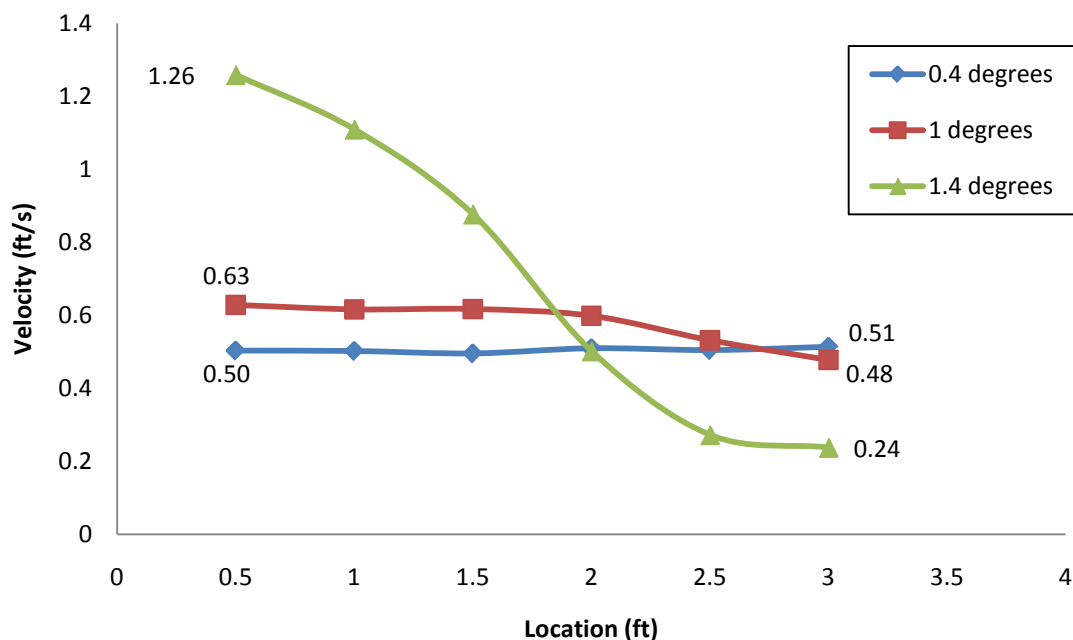
Figure 20: Velocity profile at various slopes 20 feet downstream at 800 GPM (sampling volume height (z) is 6 inches from bottom of flume).

Changing the pitch angle caused a greater destruction of an even velocity profile due to flow disturbances and uneven distribution of the water down the flume. Therefore, tilting the flume to achieve higher velocities was deemed impractical. Although at 1.4

degrees, the average velocity is appropriate for power extraction measurements, the change in velocity between the two sides of the flume is too large and flow conditions cannot be maintained.

It was determined that the friction loaded model MHK device requires a flow velocity greater than 1 ft/s to be able to spin a shaft. At the current velocity at 0° slope, the revolutions per minute of the model device were approximately 52. Doubling this amount is necessary because most small motors are rated at about 800-1000 RPM and limitations on gear reduction would only allow around 100 RPM to be effective. The uneven increase in velocity generated an unsteady hydraulic jump where different flow regimes formed upstream and downstream of the disturbance. Hydraulic jumps are described using Froude number Fr, which is a dimensionless number that defines the ratio of a characteristic velocity to a gravitational wave velocity. This is also described as the ratio of the fluid's inertia to gravitational forces. In the flume, Froude number is used to establish the resistance of an object moving through water. In this case, the Froude number upstream of the jump was greater than one (supercritical) and the downstream value was less than one (subcritical). When the Froude number is equal to one, the flow is said to be critical. The Froude number is calculated using Equation 7 for rectangular cross-sections with uniform flow depth, d (Cengel and Cimbala 2010):

$$Fr = \frac{V}{\sqrt{gd}}, \tag{7}$$

where: V is the velocity,

g is the gravitational constant, and

d is the depth of the water.

During critical flow, when the Froude number is equal to one, the inertia forces are balanced by the gravitational forces. For further testing in the flume and the development of the testing platform, the goal is to avoid hydraulic jumps and maintain a uniform subcritical flow that replicates the characteristics of a wide slow moving river in which these devices will be placed.

4.2 Flow Device to Increase the Velocity in the Flume
In order to maintain subcritical flow and avoid hydraulic jumps, several options were considered to increase the velocity of the flow. One possible option was creating an obstruction immediately after the water discharge site that would build up water behind it, then release it at a faster velocity as it cascaded over the obstruction. Another possibility was to build and install a nozzle or contraction insert which decreases the cross-sectional area of the flow, thus increasing the velocity in order to maintain a constant flow rate. The governing equations which justify the increase in velocity are outlined later in this section. This option was deemed the most practical and simple way to achieve the desired velocities in the test section. The design goals of a nozzle are to increase the velocity while maintaining flow uniformity (Ida at al. 2003). Some important parameters in nozzle design include: contraction ratio, length, and shape, which all directly affect the quality of the flow through the device (Wetzel & Arndt 1994). For example, the larger the contraction ratio the flow is more uniform and tends to have lower turbulence levels in the test section downstream of the contraction; and the length of the contraction should be short to reduce boundary layer development (Wetzel & Arndt

1994). In general, when flow is forced through a contraction, the convective acceleration of the fluid distorts the velocity profile symmetrically about the vertical centerline axis (Howes et. al 2010). Additionally, the contraction inlet should be designed to limit flow separation at the entrance by having a smooth bell-mouthed entry which will suppress turbulence and ultimately reduce velocity non-uniformity throughout the device (Walmsley 1999). The magnitude of the pressure and the spatial gradient of pressure through the contraction, if immoderate, will yield boundary layer separation (Wetzel & Arndt 1994). The nozzle insert helps to accelerate the flow and create velocities similar to that of a river environment.

4.2.1 Design Concept of the Nozzle

As a rough preliminary test to demonstrate the nozzle would work, a prototype was constructed out of plywood. Using 2 pieces of 4 feet by 8 feet plywood, 4 sets of 1.25 feet by 4 feet sections were cut and attached together using door hinges. Each piece of wood was water-proofed with deck sealant to make sure the wood would not warp. Sets of "L" brackets were mounted to the back of each of the pieces to allow for easy anchoring.

The nozzle was bolted together and anchored down using steel straps that were laid across the top of the flume and clamped down to make sure the nozzle would not float away downstream. The prototype was adjustable to nozzle exit sizes of 2 feet, 2.5 feet and 3 feet to allow for each to be thoroughly analyzed and tested before a final decision was made. A picture of the wooden prototype nozzle is shown in Figure 21.
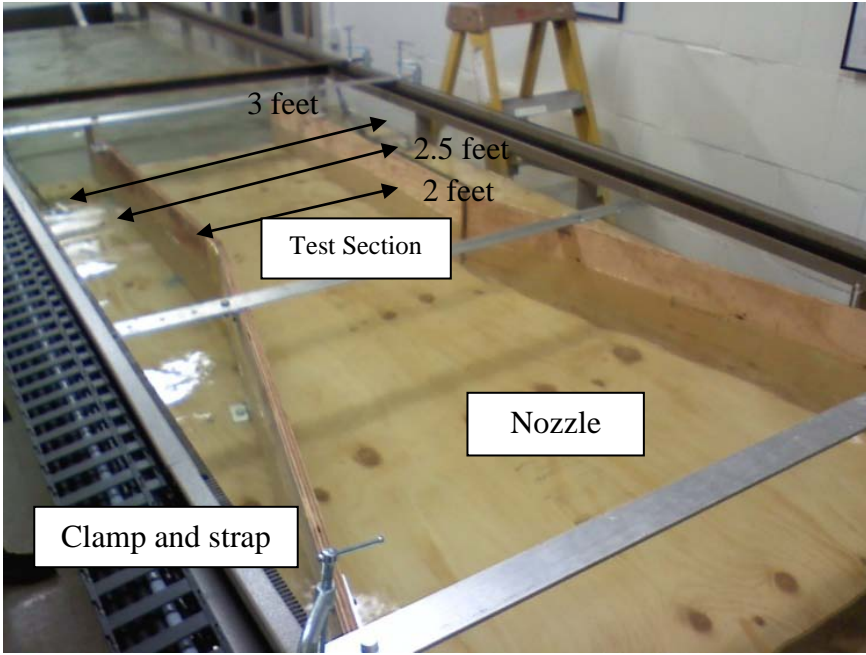
Figure 21: Wooden prototype nozzle.

Plots comparing the velocity data with the 2 feet nozzle size and without the nozzle are shown in Figure 22 at 0° slope and in Figure 23 at 1° slope. The values shown are the x-components of velocity measured by the ADV. The velocity doubles with the use of the nozzle.
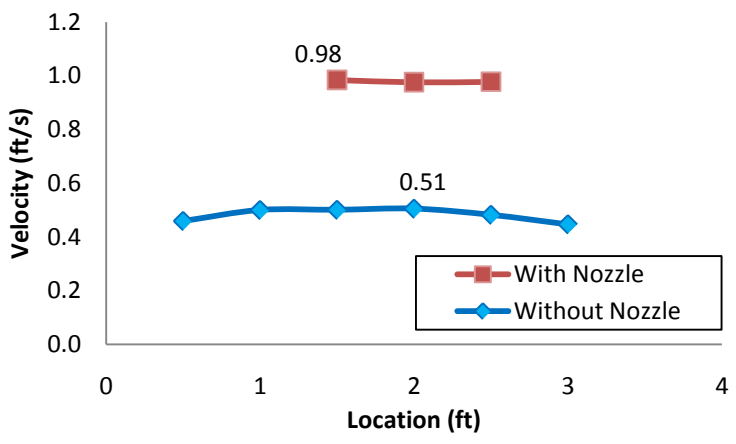
Figure 22: Velocity profile at 800 GPM 20 feet downstream with 0 degree slope (sampling volume height (z) is 6 inches from bottom of flume, 2 feet nozzle test section size).
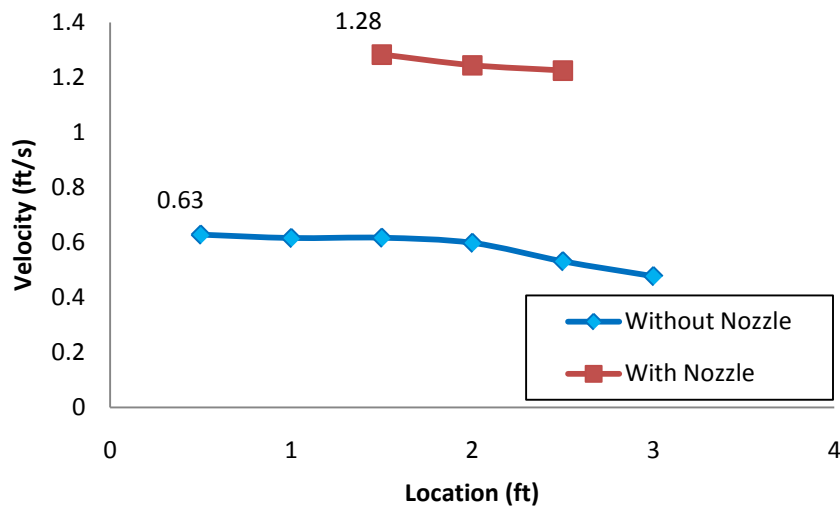
Figure 23: Velocity profile at 800 GPM 20 feet downstream with 1 degree slope (sampling volume height (z) is 6 inches from bottom of flume, 2 feet nozzle test section size).

As shown in Figure 24, the velocity in the test section of the nozzle insert increases with variations in pitch angle and an increase in flow rate.
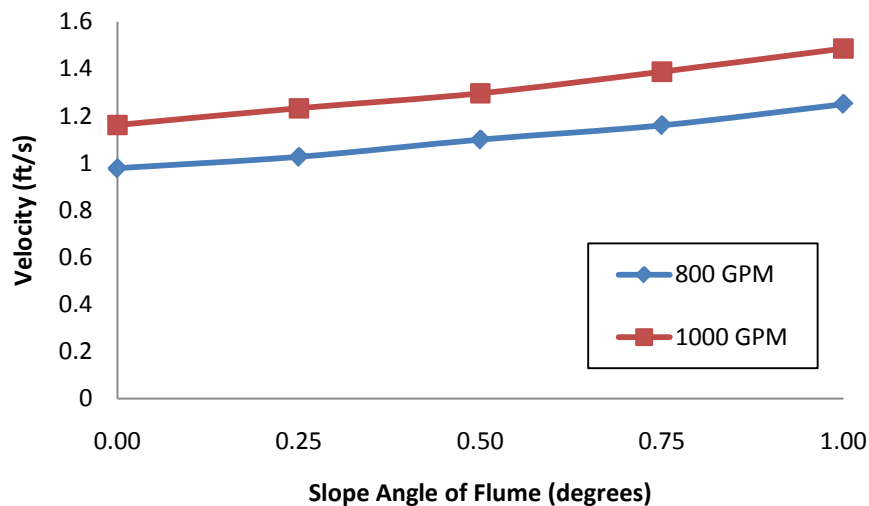
Figure 24: Nozzle prototype with 2 feet test section with varying pitch angle (sampling volume height (z) is 6 inches from bottom of flume).

4.2.2 Theoretical Description of the Flow through the Nozzle

To verify the effectiveness of the nozzle, a detailed analysis of the velocity throughout the nozzle was performed. Theoretical predictions of the velocity through the nozzle were calculated using the continuity equation. Since the flow rate through the flume is constant, the rate which the mass enters the system is equal to the rate which the mass leaves the system. The continuity equation shown in Equation 8 can be used. It "states that the time rate of change of mass within the control volume plus the net mass flow rate through the control surface is equal to zero" (Cengel and Cimbala 2010).

$$\frac{dm_{sys}}{dt} = \frac{d}{dt} \int_{CV} \rho dV + \int_{CS} \rho \, \vec{V} \, dA, \tag{8}$$

where: t is the time,

ρ is the density of the fluid,

V is the volume, and

A is the cross-sectional area.

Some of the assumptions made for the nozzle were: steady state, 1D flow, 1 inlet, 1 outlet, as well as integrating across the nozzle control volume. For this case, Equation 8 can be simplified to Equation 9 since the flow rate of the water through the flume is a constant 800 GPM.

$$\dot{V}_1 = \dot{V}_2, \tag{9}$$

where: $\dot{V}$ is the volumetric flow rate of the water, and

$\dot{V}_2$ is a point downstream of $\dot{V}_1$.

At each cross-section in the nozzle where the velocity was calculated, Equation 10 was used.

$$\dot{V} = VA \,, \tag{10}$$

where: V is the assumed integrated average velocity of the water, and

A is the cross-sectional area of the nozzle.

By using the adjustable wooden prototype, Equation 9 was tested where a decrease in cross-sectional area produces an increase in velocity to maintain a constant flow rate. After testing each option (i.e. 2, 2.5 and 3 feet test section sizes), a 2 feet nozzle test section size was deemed the optimal size by meeting required water velocity for power extraction studies and allowing room to mount the model MHK device or other cylinders in the test section. Preliminary testing with the nozzle in place was done at a 2 feet nozzle test section size at both 800 and 1000 GPM while varying pitch angle to understand how velocity would change (see Figure 24).

4.2.3 Design of the Permanent Nozzle Insert

Using the preliminary data from the wooden contraction, a permanent nozzle insert for the flume was designed. The nozzle was designed to fit with the existing sediment bed insert and allow the 3D positioning device situated along the top of the flume to which the ADV probe is mounted to traverse overtop the insert. The fabrication and construction of the nozzle insert was done in the Project Development Lab (PDL) in the Dana Engineering building. Final specifications for size and shape for a permanent nozzle insert were created based on the dimensions of the existing sediment bed insert.

In a paper by Howes, Burt and Sanders in 2010: "The subcritical contraction walls and floor should be relatively smooth. The height of the contraction should be set with sufficient freeboard so that overtopping does not occur…The floor of the contraction should be at the same elevation as the existing channel bed" (Howes et al. 2010). The design was modeled using Pro/Engineer to ensure the nozzle would fit in the flume in conjunction with the sediment bed insert. Materials for the nozzle, polyethylene and acrylic, were chosen based on their smoothness and low cost. The bottom of the nozzle follows the incline of the ramp of the sediment insert to maintain a constant elevation leading into the test section. Further improvements were made from the initial wooden prototype including a curved entry, a transparent test section and a diffusing section. The diffusing section of the contraction decelerates the flow after passing through the test section and prevents any unwanted swirling or wall effects from stagnant water lying on the outer sides of the test section. The nozzle was designed to sit flush with the maximum height of the flume, maintaining a constant height of 15 inches. This prevents overtopping from occurring. The entry of the nozzle is curved following an equation used in the construction of low speed wind tunnels. The curve helps to prevent separation of the flow along the walls as it enters the test section by use of two curves combined at an inflection point located 30 inches from the entrance of the nozzle (Watmuff 1986). For best results, "a contraction should be designed to prevent flow separation along its walls and also to minimize exit plane boundary layer thickness and flow non-uniformity" (Doolan 2007). The fifth-order polynomial equation used to define

the curvature is shown in Equation 11 with the only controllable parameter being the overall length of the contraction (Doolan 2007).

$$h = (-10\xi^3 + 15\xi^4 - 6\xi^5)(h_i - h_o) + h_i \tag{11}$$

where: h is the distance from the centerline of the flume,

ξ is the position of the contraction walls normalized over the length of the contraction (x/L),

x is the distance from the contraction inlet, and

L is the overall length of the contraction.

Shown in Figure 25 is a schematic of the shape of the walls and the path of the water through the nozzle as it contracts from 4 feet to 2 feet.
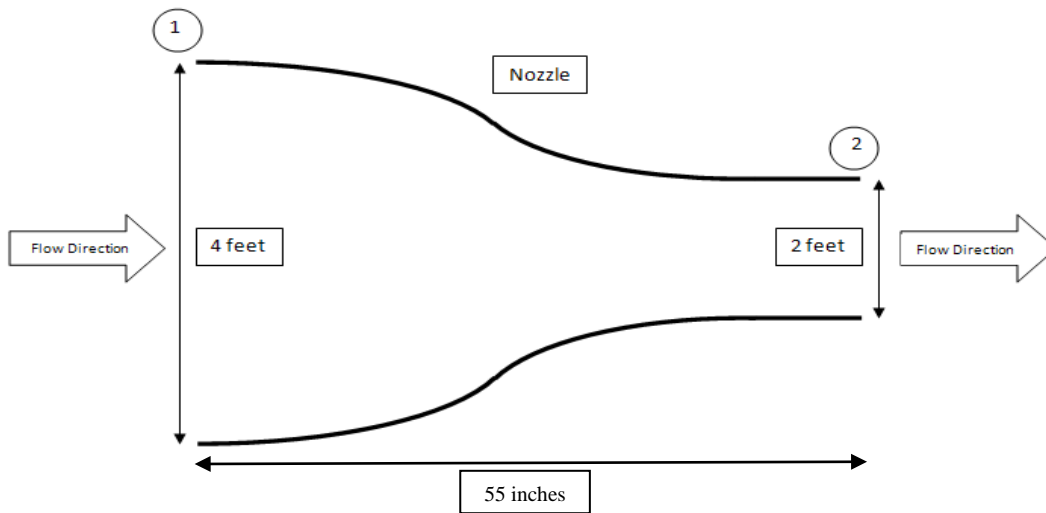
Figure 25: Representation of nozzle concept and design.

To build the curves, flexible 1/8 inch polyethylene was used to follow the contour of the more rigid ½ inch polyethylene. The thicker polyethylene was marked and cut using a jigsaw to make sure the desired curve was followed.

Since the existing sediment bed insert rises to a 3 inch height over a 55 inch span, the contraction portion of the nozzle followed this feature to maintain a consistent 15 inch height leading into the test section so the traversing gantry can freely move along the length of the flume. An overhead picture of the permanent nozzle and sediment insert can be seen in Figure 26.
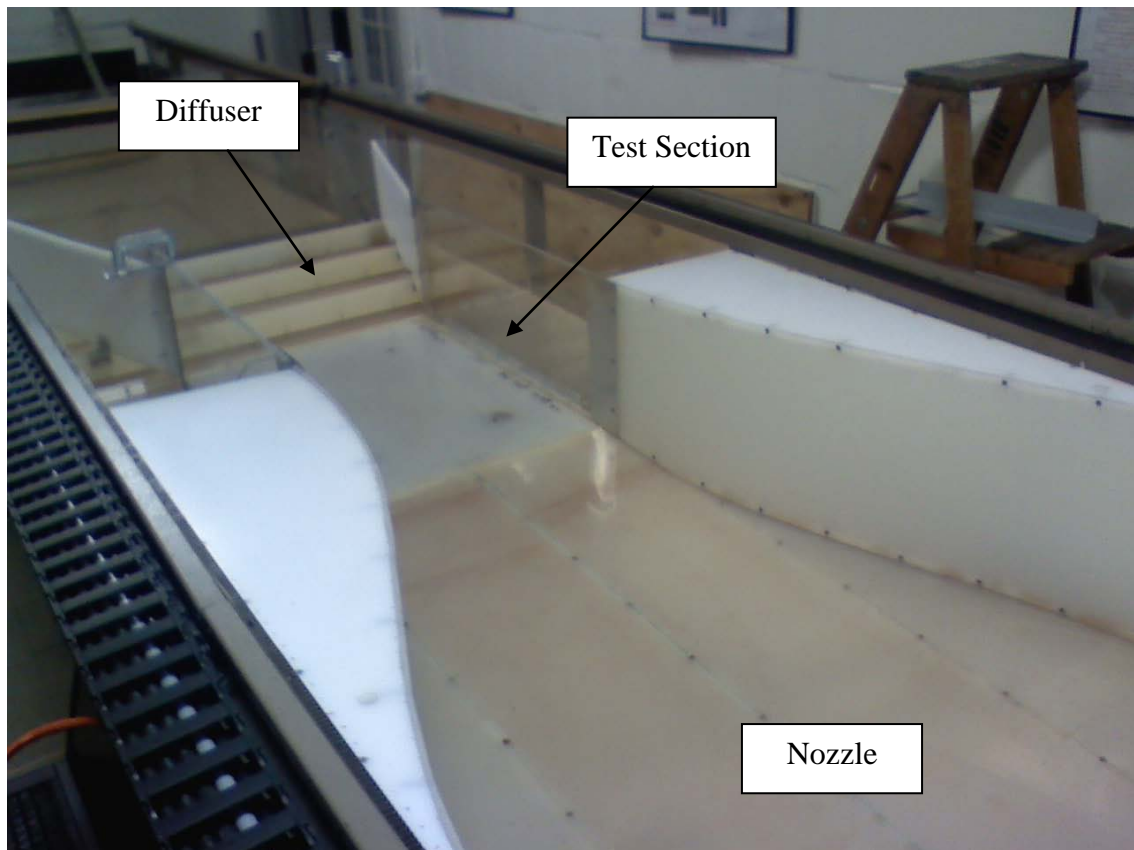
Figure 26: Overhead picture of the permanent nozzle.

The test section was made using transparent acrylic for easy visualization of the flow so optical diagnostic instrumentation such as a Particle Imaging Velocimetry (PIV) system can be used. The pieces were cut to a size 1 foot tall by 2 feet wide to span the entire distance of the test section. Triangular pieces of acrylic were cut as perpendicular support structures and were anchored to the insert using 'L' brackets with holes in which screws were drilled. A picture of the 'L' shaped support brackets can be seen in Figure 27.
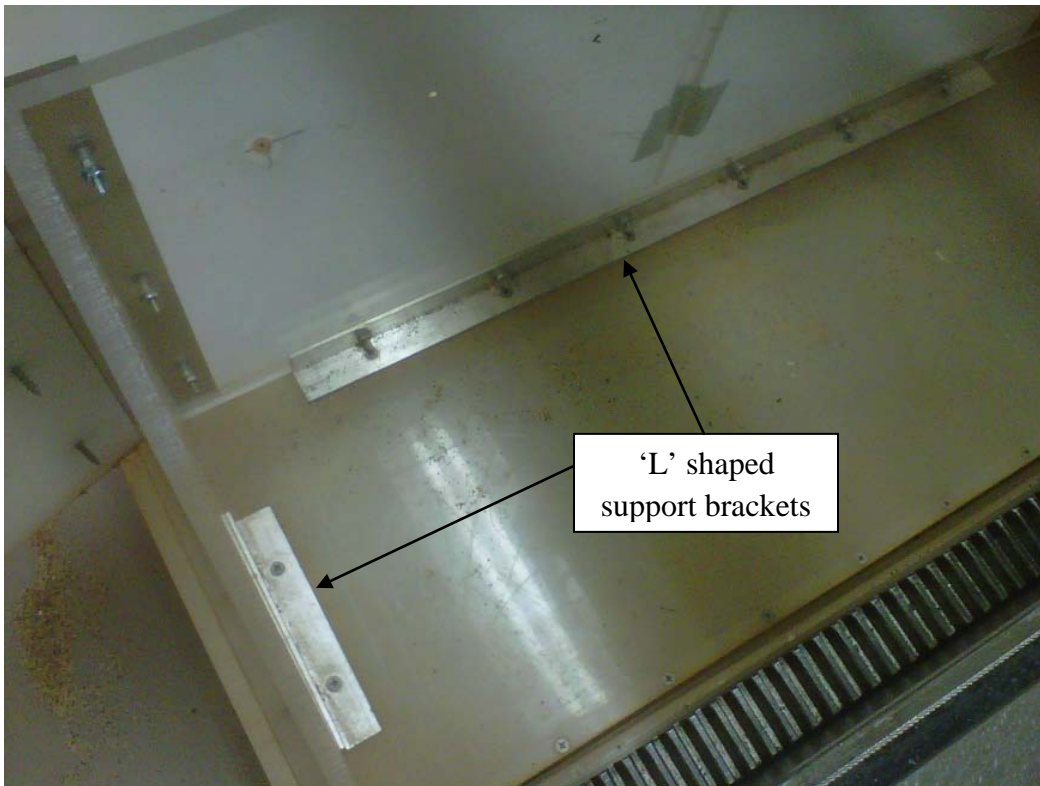
Figure 27: Overhead view of support brackets of acrylic pieces.

Using pieces of ½ inch polyethylene, the diffusing section was made by cutting 1 foot tall by 3 feet wide sections that are anchored to the sediment insert by use of 'L' brackets on both the insert and diffuser pieces (shown in Figure 28). The use of the

diffusing section prevents flow separation which would occur if the contraction abruptly stopped after the test section.   Flow separation is the process in which when "a fluid is forced to flow over a curved surface, such as the back side of a cylinder, the boundary layer may no longer remain attached to the surface and separates from the surface" (Cengel and Cimbala 2010). In the case of the test section and the diffuser, vortices shed by the walls of the nozzle could contaminate the flow in the test section. The fast flowing water meeting the stagnant water sitting outside the test section would cause flow disturbances that would propagate upstream into the test section and possibly skew experimental results.   The diffusing section guides the water out of the test section without inducing any disturbances upstream.

'L' shaped mounting bracket

Figure 28: Mounting brackets for diffusing section of nozzle.

4.2.4 Velocity Data through the Nozzle

Experimental values for the velocity in the nozzle were taken using the ADV probe. The nozzle was divided into five sections, 12.375 inches apart in the axial direction starting from the beginning of the nozzle. A total of 26 points were measured and each row was averaged to find the mean velocity across the width of the flume section. The sampling volume height was maintained at a constant six inches from the ramp for each of the points. The location of the measured velocity values can be seen in Figure 29. The calculated theoretical values using Equation 9 are shown in Table 2. Figure 30 shows the increase in velocity as the water moves through the nozzle. Due to limitations of the 3D positioning device, locations farther than three feet from the wall in the transverse direction could not be measured. These measurements were done before the sluice gate and honeycomb straightener were added to the flume. As observed in Figure 29, close to the exit of the contraction at the boundary, an overshoot of velocity occurs. This is accompanied by a drop in boundary pressure and has also been reported in recirculating water tunnel contraction data (Wetzel & Arndt 1994).
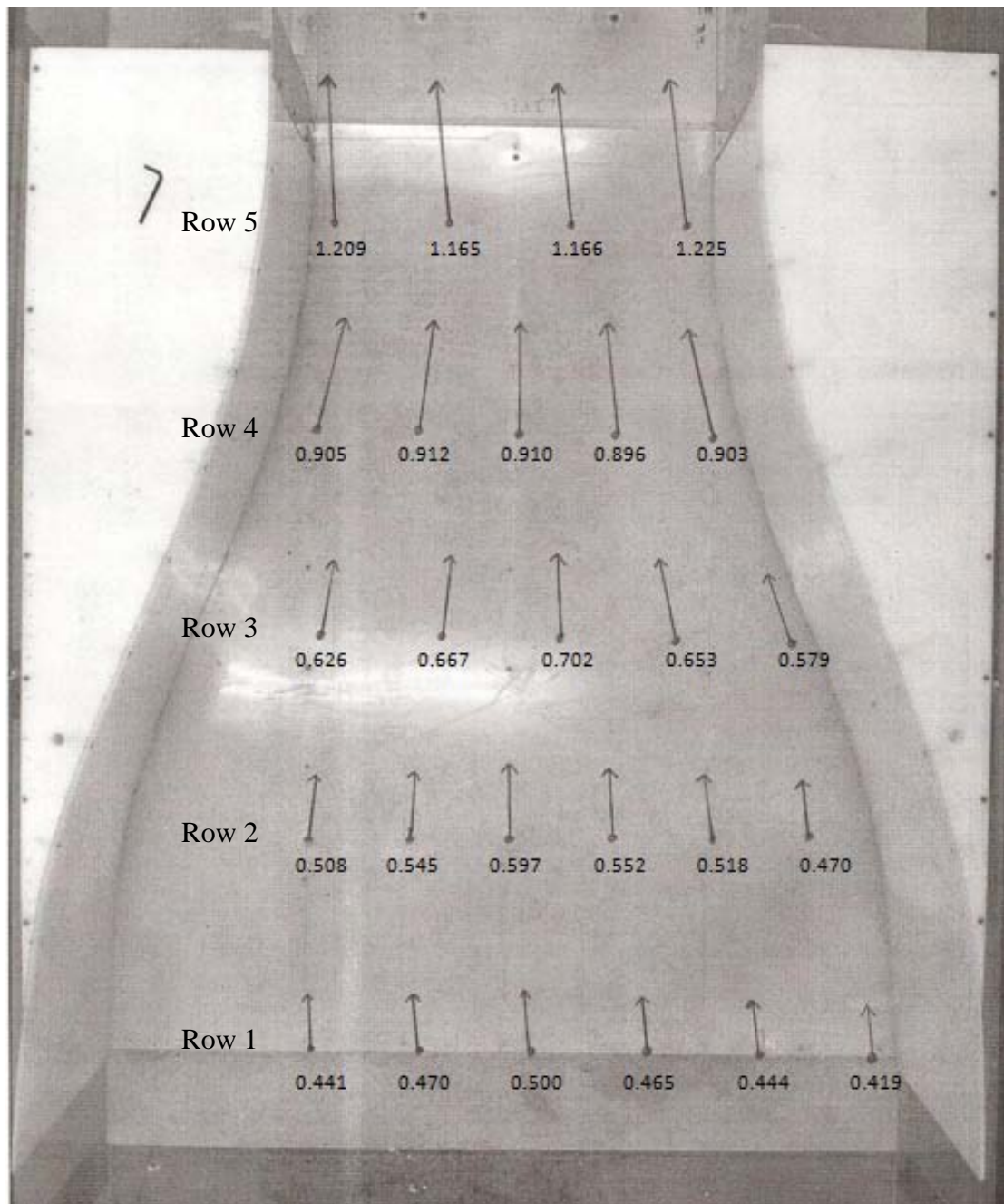
Figure 29: Overhead photo of nozzle with scaled velocity vectors at measurement points (all values in ft/s, only x- and y-components used for velocity vectors).

Table 2: Theoretical values at the first five rows in the nozzle using Equation 10 (assuming 12 inch water height).

Row	Location relative to start of nozzle (in)	Height of water relative to height of insert (in)	Width of nozzle (in)	Area (ft^2)	$V_{theoretical}$ (ft/s)	$V_{experimental}$ (ft/s)
1	0.00	11.50	47.50	3.79	0.47	0.46
2	12.38	11.13	45.00	3.48	0.51	0.53
3	24.75	10.51	37.25	2.72	0.66	0.65
4	37.13	9.89	27.75	1.91	0.94	0.91
5	49.50	9.28	24.00	1.55	1.15	1.19
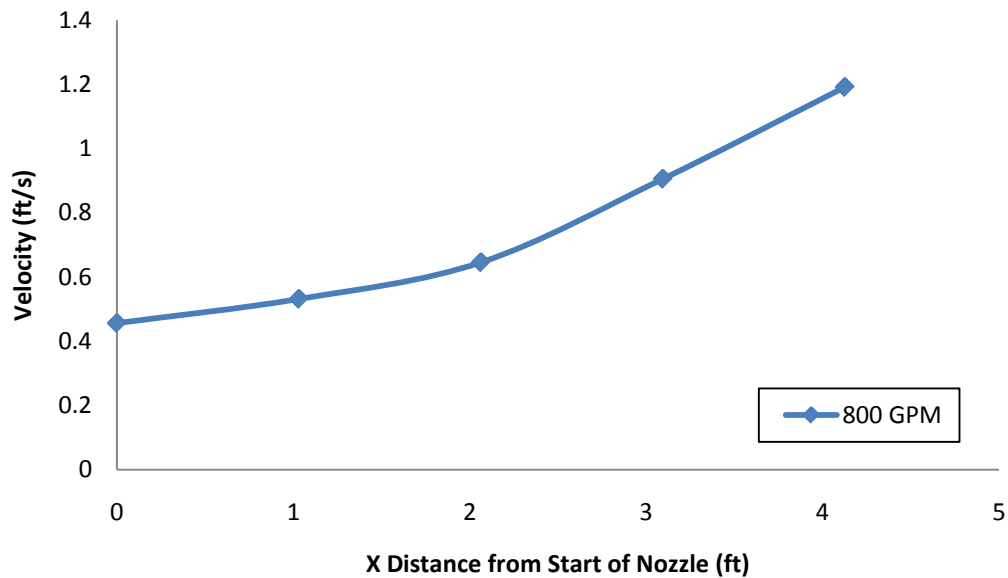
Figure 30: Graphical representation of the increase in velocity in the nozzle.

4.3 Measurement Methods to Predict Scour and Erosion

Due to the presence of model MHK devices which obstruct the flow, scour and erosion patterns form along the sediment bed which is analyzed using an HR Wallingford 2D bed profiler. This bed profiler is capable of yielding bed form topology in a laboratory setting which will provide insight into how actual river beds respond to the addition of hydrokinetic devices. Additionally, results from tests done with the profiler provide preliminary data on the optimal design of support structures for the devices. The basic concept of sediment scour around structures in flows can be seen in Figure 31.
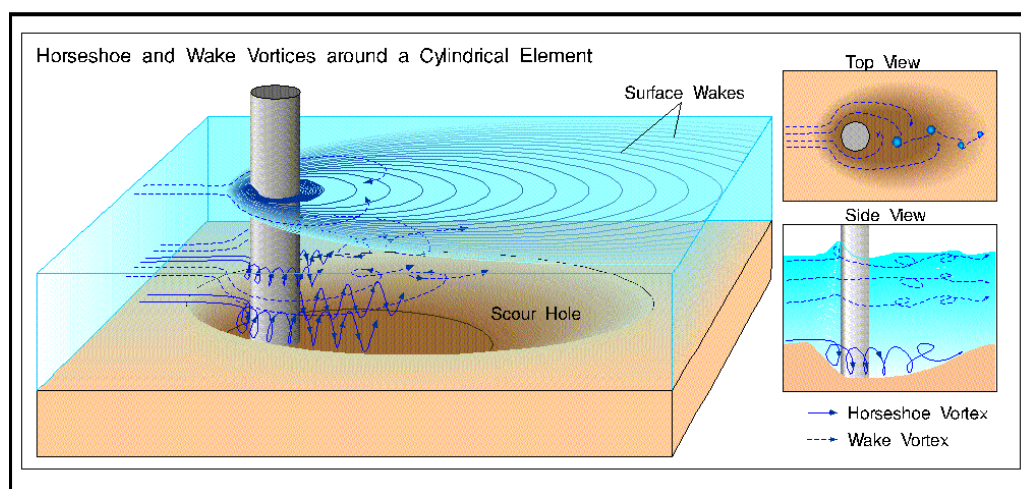
Figure 31: Drawing of sediment displacement around a cylindrical element (adapted from Sandia National Laboratories).

4.3.1 Initial Tests with a Point-Gauge

Collecting data to estimate scour rates or bed form topology can be done in many ways. Before receiving the 2D bed profiler, bed form topology was generated using a point-gauge attached to the gantry. The point-gauge was zeroed at the base of the test section and the height of the sediment was measured as a delta or difference from the zero condition. A portrayal of the erosion of the sand in the test section after five minutes

of running water is shown Figure 32. Although a sieve analysis was done on a coastal

sand sample, not enough sand was available to fill the test section. For this experiment,

Red Flint Filter and Industrial sand was used for preliminary testing. A close-up picture

of the scour around the cylinder is shown in Figure 33. A 2D graphical result of the data

using the point gauge is shown in Figure 34. The 3D results using the point gauge are

shown in Figure 35.

Figure 32: Sediment in test section.

Figure 33: Erosion around cylinder in test section.
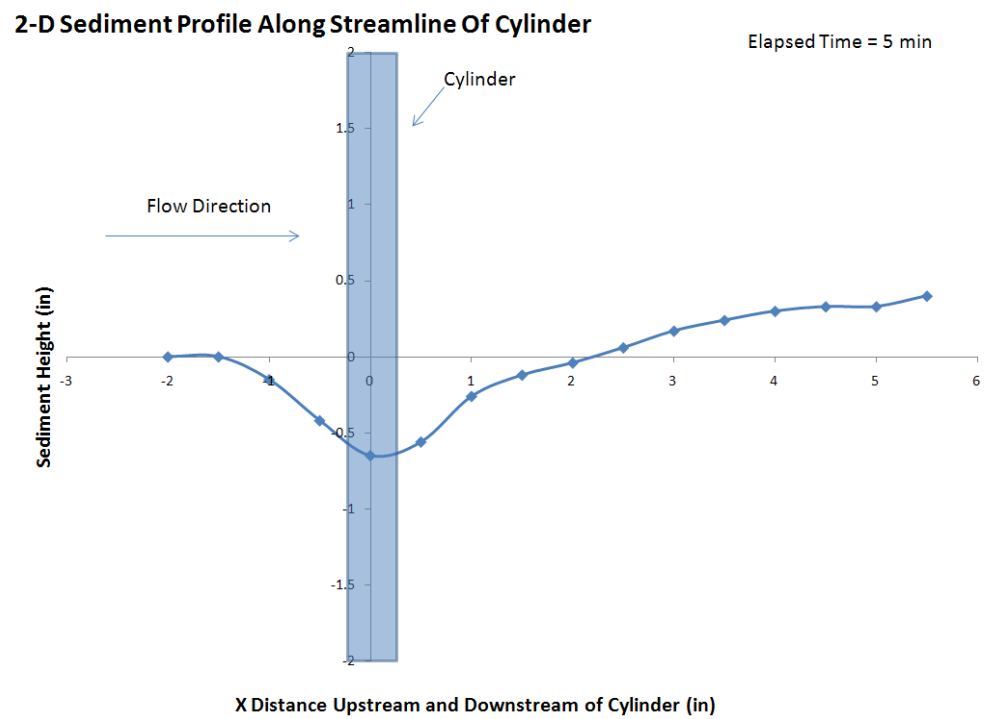
Figure 34: 2D sediment profile across a cylinder.
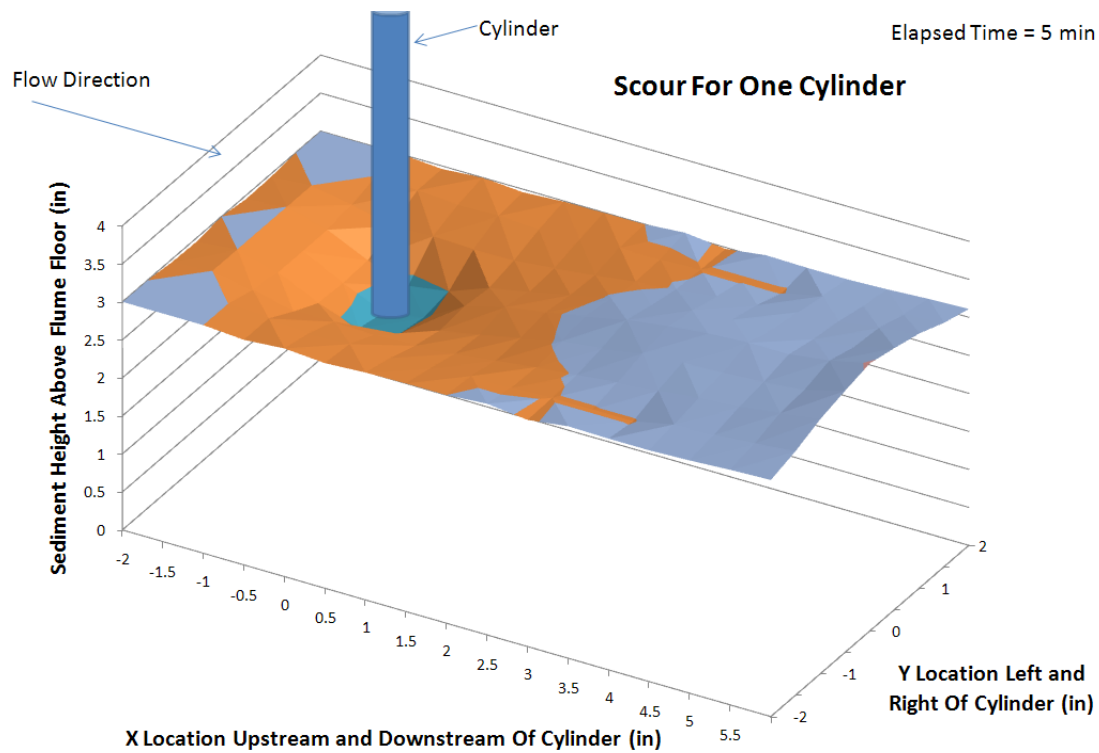
Figure 35: 3D sediment profile across a cylinder.

4.3.2 2D Bed Profiler System

Using the capabilities of the HR Wallingford 2D profiler, topographical plots of the bed form were constructed. Upon receiving the 2D profiler, the system was set-up and the profiler was placed into the flume to be tested to ensure the system operated properly. The track, traverse and laser probe are shown in Figure 36.
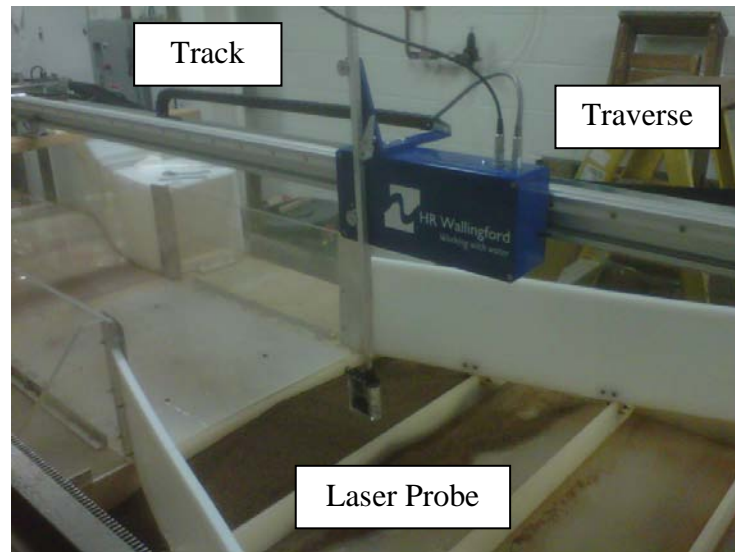
Figure 36: HR Wallingford Sediment Profiler.

The track of the profiler was bolted to two 4.5 feet long sections of 2 inch by 4 inch wood. The wood pieces straddled across the width of the flume and were anchored using C-clamps. This set-up can be seen in Figure 37.

Figure 37: Preliminary set-up.

The traversing system moves along the track using a gear on a motor that works like a rack and pinion system. Another motor connects to the track on the laser probe by way of a similar rack and pinion device as shown in Figure 38. The probe is held onto the motor by two gears and a passive spring which create three points of contact to hold the probe in place. The probe plugs into the top of the motor and then through a second cable which sends the data to a connected central hub that then connects to the computer.

Figure 38: Traversing system.

4.3.3 Tests with the 2D Profiler

Initial testing using the sediment profiler yielded the data shown in Figure 39. This testing was done without sediment to see how the system would perform. The probe was zeroed behind the diffusing section of the nozzle sediment insert and was set to run across the three baffles of the sediment collecting area. Since the flume and insert are made of Plexiglas and polyethylene, respectively, the laser passed through the material until it hit the metal support bracing underneath it. This explains the negative starting

value and the negative baseline values as the probe traversed the three baffles. Figure 40

shows the location of where the initial test was taken.
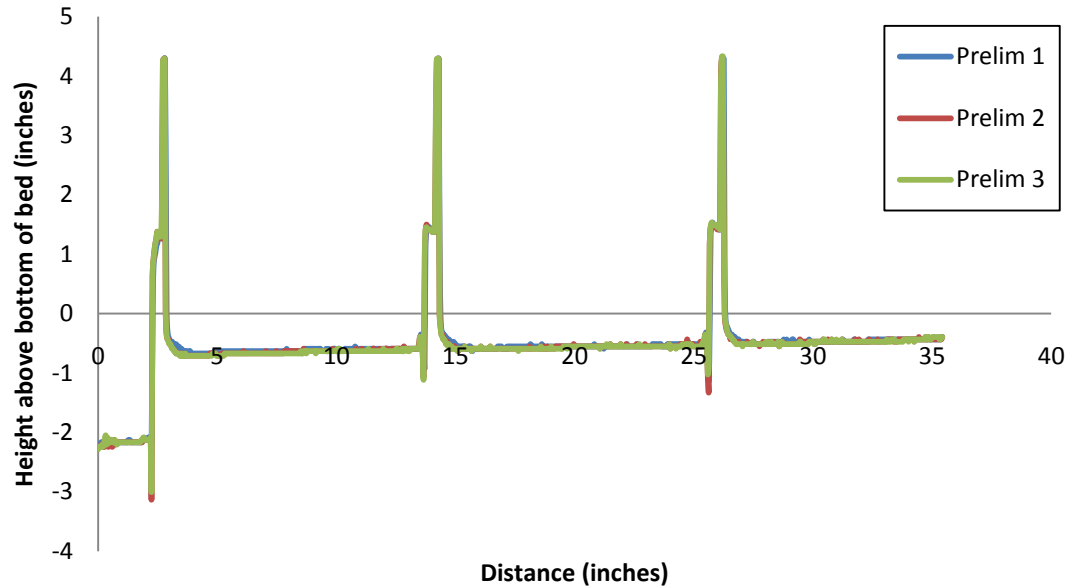
Figure 39: Preliminary profiler testing.
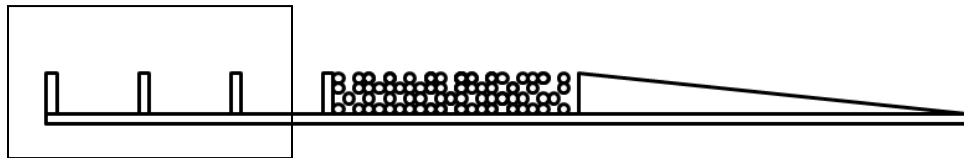
Figure 40: Location of initial profiler testing.

After encountering errors without sediment due to the material of the flume and

insert, sand was placed in the first of the three baffles to see how the touch probe would

traverse across the section. The flume was run for 2 hours and the sediment in the baffle

was profiled. A picture of the actual sediment is shown in Figure 41. The red line on the

photograph shows the contour of the top of the sediment where the data was taken. The

plot produced by the sediment bed profiler is shown in Figure 42. A total of 58 data

points were taken every 0.2 inches along the length of the baffle for approximately 11 inches.

Figure 41: Eroded sediment in baffle (red line indicates top of sediment).
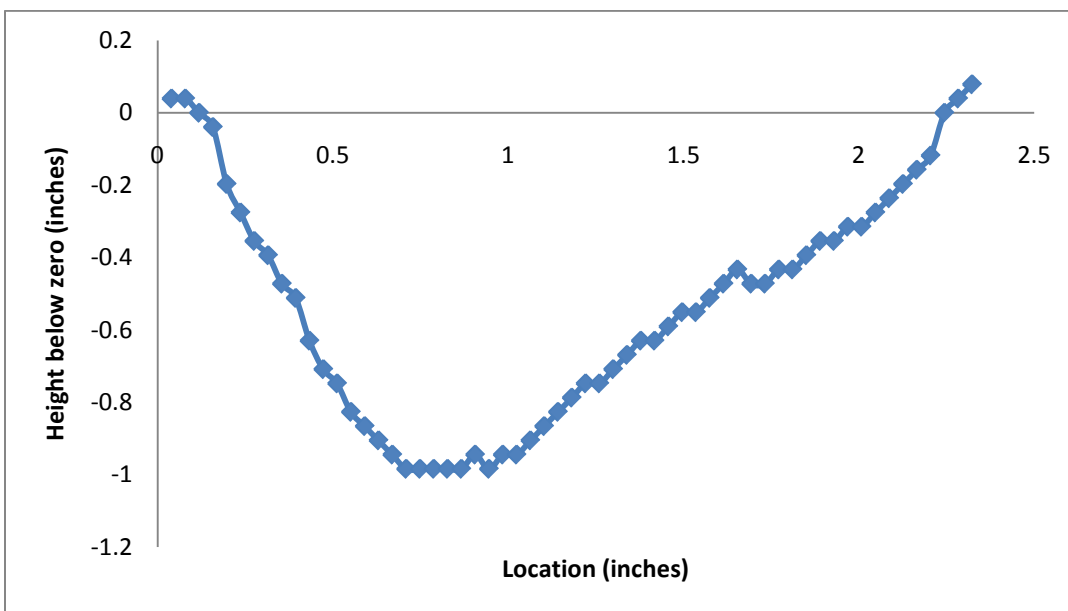
Figure 42: Sediment displacement plot with touch probe.

To determine the amount of sediment displaced by scour and erosion, a method based on Riemann sums was developed to use the data provided from the bed profiler. Since the distance (step value) between each point on the plot is approximately 0.2 inches, the height is multiplied by the step value to create a series of rectangular areas. These 58 rectangles were added together to produce an approximate total area. The approximate amount of sediment displaced, assuming a perfectly level initial condition of the bed, is 6.39 inches^2. This only accounts for one profile across the length of the baffle out of infinitely many cross-sections of the sediment bed. With a new permanent mounting system for the bed profiler, the distance between each profile across the width of the flume will be used to determine a volume of displaced sediment. With this information, scour rate can be determined using the volume of displaced sediment along with the period of time needed to move the sediment.

4.4 Baseline Reference Conditions of the Hydraulic Flume

With both the sediment and contraction inserts in place, test results verify baseline reference conditions after theoretical calculations and data analysis are conducted. Data for multiple flow discharge rates is used as a comparison for studies performed in the future. Two new conditioning devices were added in an attempt to create a more constant velocity profile across the width of the flume. A sluice gate was added following the water discharge site about 3 feet downstream. A honeycomb was also added 1.5 feet downstream of the sluice gate. A schematic of the full flume with the components in place along with the nozzle sediment insert and tailgate is shown in Figure 43.
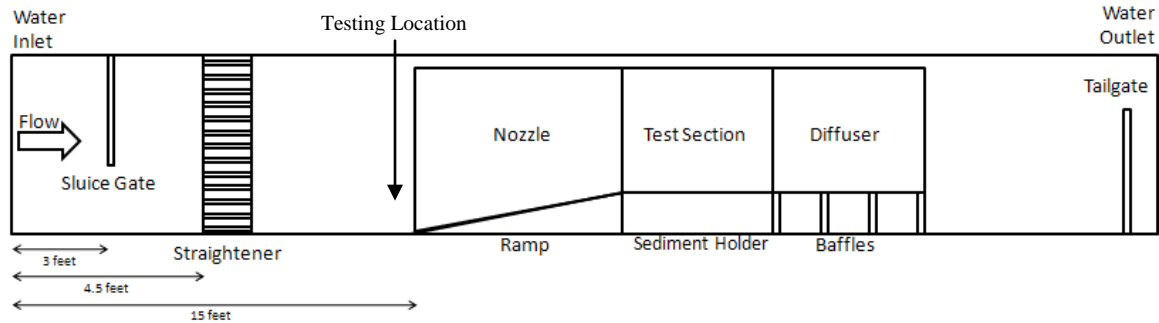
Figure 43: Full flume schematic (not to scale).

Having these new conditioners along with the nozzle sediment insert, it was necessary to measure a velocity profile across the width of the flume at a location after the sluice gate and straightener to understand the effects it has on the flow. This allows for baseline reference conditions to be documented for later use. When future testing is being done, these conditions can be referenced to make backwater calculations and determine energy losses when the model MHK device is in place based on components upstream of the test section.

A location prior to the nozzle was chosen to take measurements for the velocity following the flow conditioning devices. The approximate location is shown in Figure 43. The velocity measurements were taken at six points across the flume starting 6 inches away from the origin and moving in the transverse direction in increments of 6 inches until reaching a distance of 3 feet. Each set of six points were taken at three different z-locations: a sampling volume location of 5.5, 7.5 and 9 inches from the bed (bottom) of the flume. Each set of measurements was made for a flow rate of 700, 800 and 900 GPM. Each point was taken for a 5 minute interval at a sampling rate of 10 Hz using the ADV probe. Figure 44 shows the basic shape of a velocity profile of a turbulent flow

over a flat plate. The velocity, u, is used to describe the flow. There is a no-slip condition at the bottom boundary where the fluid is bounded by the wall, u(Z=0)=0. At the free surface, the flow reaches a maximum velocity defined as u(Z=12) = U_∞. The data from the experiment is shown in Table 3. A velocity profile plot similar to what is illustrated in Figure 44 was observed in the data through an increase in velocity with depth.
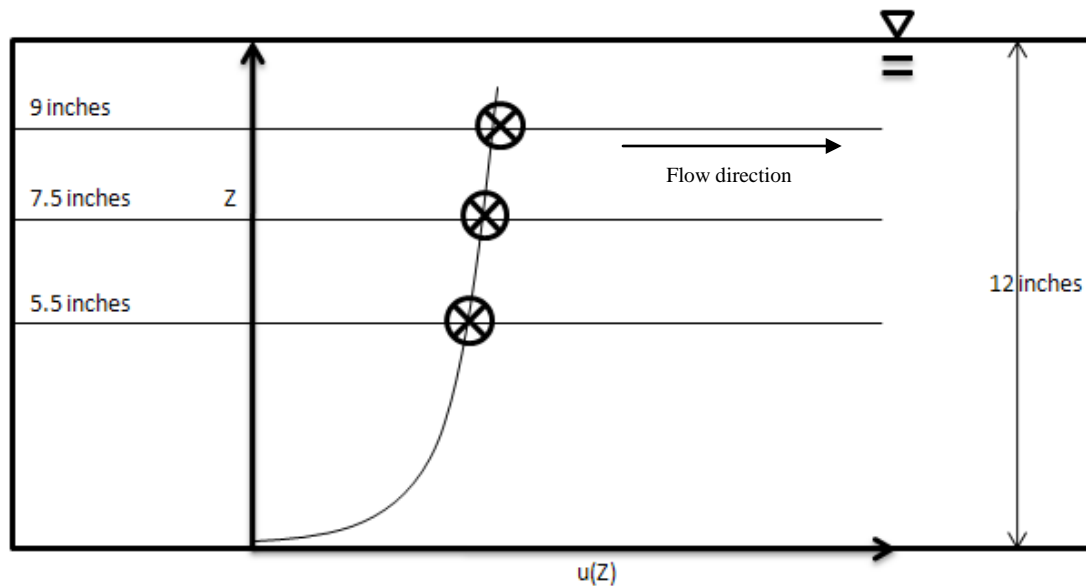
Figure 44: Schematic of a turbulent velocity profile.

Figure 45 shows a non-dimensionalized plot of the boundary layer at the beginning of the nozzle to support the presence of a turbulent boundary layer. Points were taken at a sampling volume starting at the bottom of the flume and increased in the z-direction at a 1/8 inch interval. A total of 81 points were measured. Z/δ is the non-dimensionalized height of the sampling volume and u/U is the non-dimensionalized velocity. The magnitude of velocity, U, is used "as the characteristic velocity scale for

boundary layers" (0.45 ft/s) while the length scale, δ, (10 inches) is the distance normal to the streamwise direction with respect to Z (Cengel and Cimbala 2010). The curve $Z/\delta^{(1/2)}$ represents the laminar boundary layer while the transition to turbulence occurs at $Z/\delta^{(1/7)}$ based on the Blasius laminar boundary layer solution, which is defined by the one-seventh-power law (Cengel and Cimbala 2010). The actual data set most closely follows the $Z/\delta^{(1/8)}$ curve. Since the one-seventh-power law states that anything above one-seventh is turbulent, the flow at the beginning of the nozzle can be assumed to be turbulent flow.
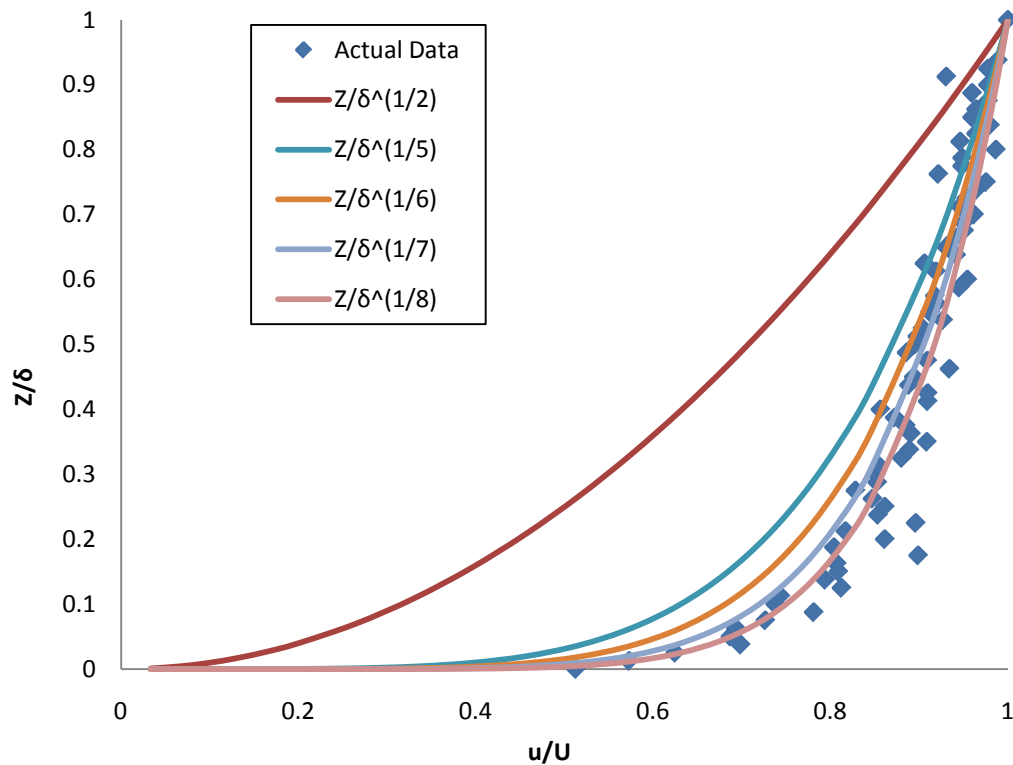

Figure 45: Non-dimensionalized turbulent boundary layer.

Table 3: Velocity (ft/s) across width of flume after sluice gate (x-component of velocity).

	Location along y-direction (ft)							
Flow Rate	0.5	1	1.5	2	2.5	3	Avg Velocity (ft/s)	Height (inches)
	0.432	0.446	0.429	0.412	0.382	0.403	0.417	5.5
700 GPM	0.448	0.453	0.446	0.415	0.412	0.429	0.434	7.5
	0.469	0.474	0.456	0.417	0.426	0.456	0.450	9
	0.483	0.486	0.472	0.448	0.429	0.447	0.461	5.5
800 GPM	0.486	0.494	0.484	0.452	0.477	0.493	0.481	7.5
	0.519	0.532	0.501	0.48	0.479	0.521	0.505	9
	0.52	0.503	0.51	0.494	0.484	0.536	0.508	5.5
900 GPM	0.535	0.509	0.508	0.492	0.542	0.523	0.518	7.5
	0.547	0.537	0.536	0.504	0.498	0.58	0.534	9

The plot in Figure 46 shows the height of the sampling volume versus the average velocity across the width of the flume. As the flow rate increases, the average velocity in the profile increases. The velocity profiles in Figure 46 do not exactly follow the turbulent velocity profile shown previously, but this variation can be attributed to the values being an average across the width of the flume.
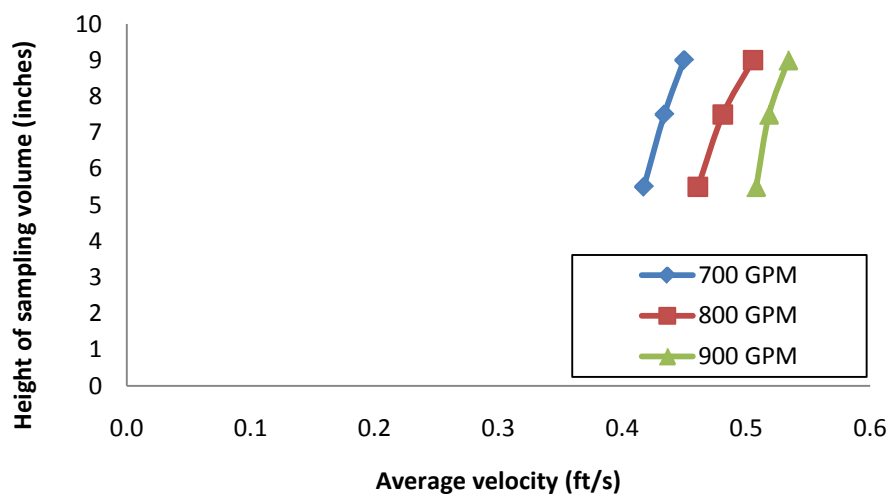
Figure 46: Varying sampling volume height at different flow rates (x-component of velocity).

With the sampling volume at a height of 5.5 inches from the bed of the flume, the velocity profile at the three different flow rates are shown in Figure 47. The velocity profile across the flume stays fairly consistent without any outlying velocity points.
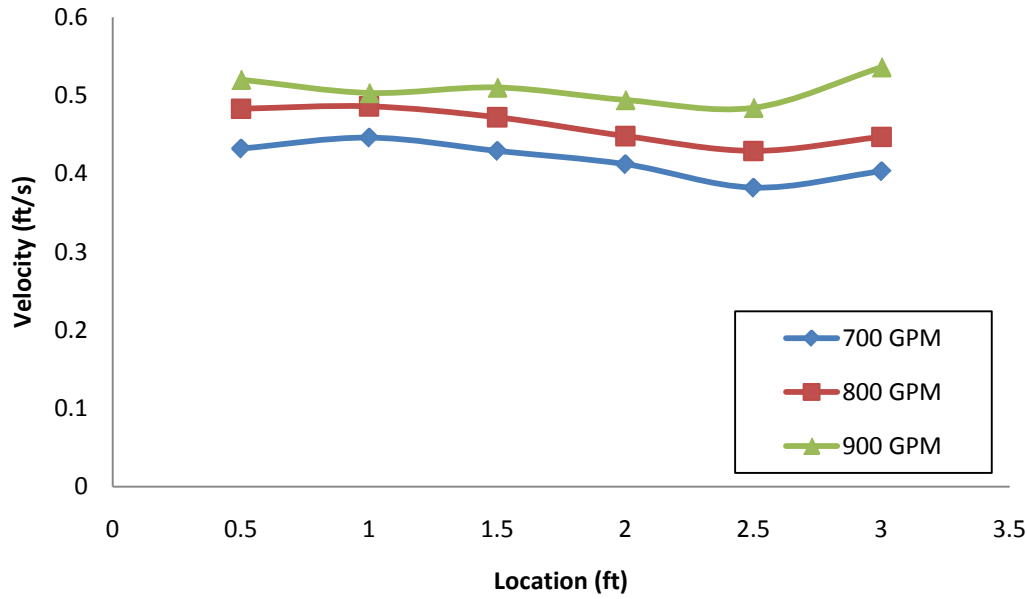
Figure 47: Velocity profile at 5.5 inch sampling volume height (x-component of velocity).

To prove the effectiveness of the sluice gate and straightener, energy calculations were completed using the mechanical energy equation to ensure that the velocity of the water after the flow control devices was faster with minimal head losses. For a steady, incompressible flow, the total mechanical energy of a liquid is given as (Cengel and Cimbala 2010):

$$H = y + \frac{V^2}{2g} + S_o x, \tag{12}$$

where: H is the energy,

y is the pressure head in an open channel flow,

x is the location along the length of the flume,

g is the acceleration due to gravity,

V is the velocity of the liquid, and

$S_o x$ is the elevation of the bottom of the flume (S_o is the slope).

Modifying Equation 12, the energy upstream and downstream of the sluice gate and straightener was calculated using the energy equation (Equation 13) where section 1 is a point upstream of the sluice gate and section 2 is a point downstream:

$$S_o x_1 + y_1 + \frac{V_1^2}{2g} = S_o x_2 + y_2 + \frac{V_2^2}{2g} + h_L, \tag{13}$$

where: h_L is the head loss across the flow conditions.

Figure 48 shows the control volume where Equation 13 was used with (1) being upstream of the sluice gate and (2) being downstream of the straightener.
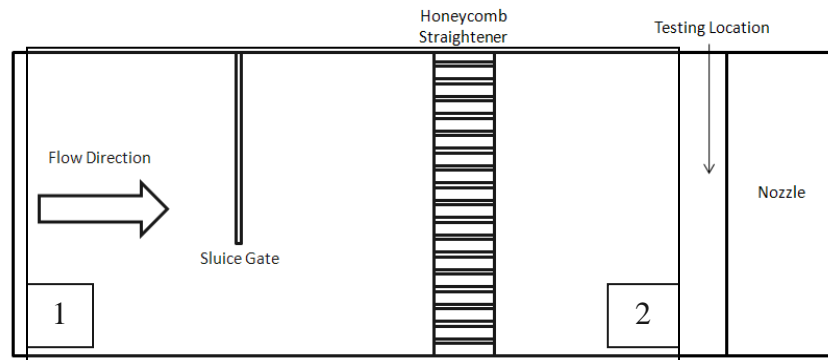
Figure 48: Sluice gate control volume (1 is upstream of sluice gate, 2 is downstream).

Table 4 shows the values of flow rate, velocity, water flow depth and head loss upstream and downstream at each of the three flow rates tested. For all three flow rates

the flume was at a slope of zero ($S_o = 0$). Upstream and downstream water depths were measured for each flow rate. The average upstream velocities were calculated using Equation 10 while the average downstream velocities were measured using the ADV. These values were then used in Equation 13 to calculate the head loss between the upstream and downstream locations.

Table 4: Head losses involved in use of sluice gate.

Flow Rate (GPM)	700		800		900	
Location	Upstream	Downstream	Upstream	Downstream	Upstream	Downstream
Elevation (ft)	3.27	3.27	3.27	3.27	3.27	3.27
$S_o x$ (ft)	0	0	0	0	0	0
Flow Rate (ft^3/s)	1.560	1.734	1.783	1.990	2.006	2.166
V_{avg} (ft/s)	0.371	0.434	0.411	0.482	0.446	0.520
Flow Depth (ft)	1.052	1.000	1.083	1.031	1.125	1.042
Head Loss (ft)	0.000	0.051	0.000	0.051	0.000	0.082
Energy Head (ft)	1.054	1.003	1.086	1.035	1.128	1.046

The energy curves for each respective flow rate (700, 800 and 900 GPM) are shown in Figures 49, 50, and 51, respectively. The energy curve is created using the upstream and downstream flow rates and water heights of the control volume as well as the width of the channel. The MATLAB program used to create these curves is attached in Appendix I. The solid line on the plot represents the energy before the sluice gate at point 1 and the dotted line represents the energy downstream at point 2 as shown in Figure 48. The vertical difference between points 1 and 2 in Figure 49 is the change in water height and the horizontal difference is the loss of energy (head loss) due to the

sluice gate and straightener. All values on the curves below the critical depth are supercritical while all values above the critical depth are subcritical.
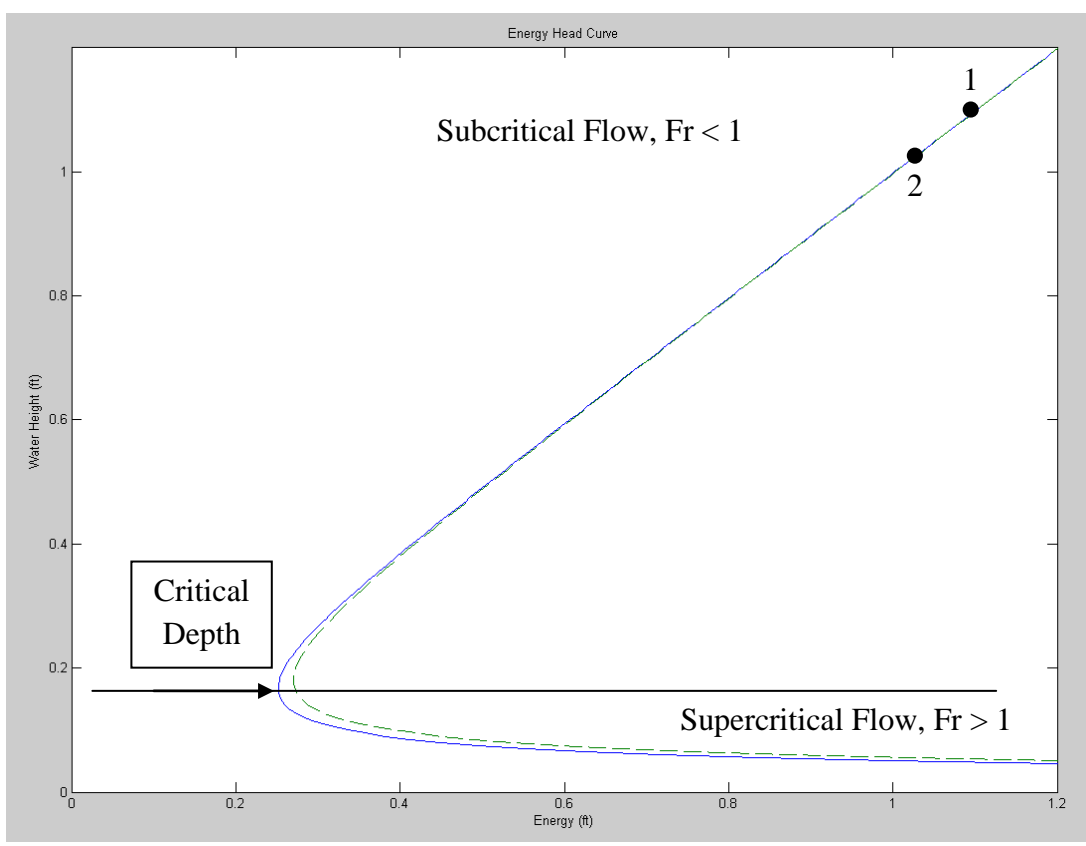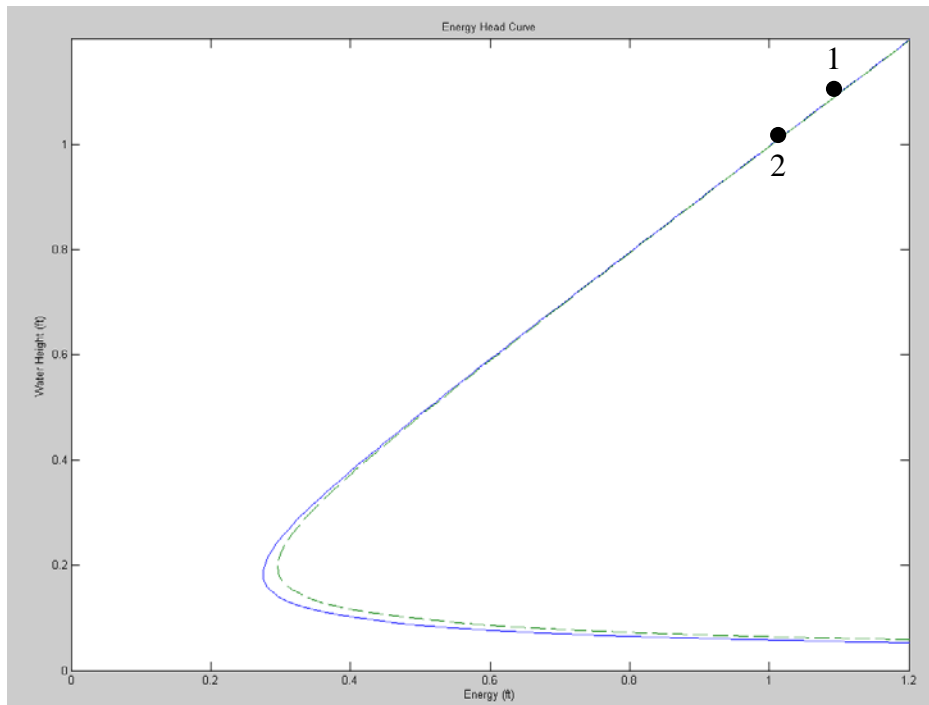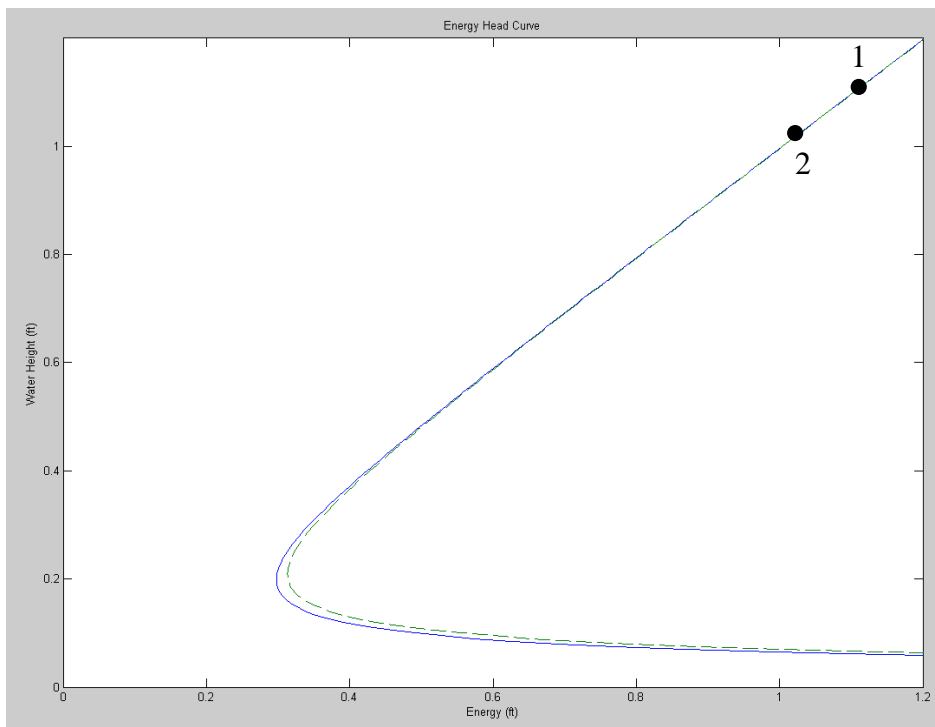

Figure 49: 700 GPM energy curve (using velocity and water height data from control volume of sluice gate and straightener).

Figure 50: 800 GPM energy curve (using velocity and water height data from control volume of sluice gate and straightener).

Figure 51: 900 GPM energy curve (using velocity and water height data from control volume of sluice gate and straightener).

At flow rates of 700 and 800 GPM, the head loss across the flow conditioner is approximately 0.051 feet. For a flow rate of 900 GPM, the loss in energy is approximately 0.082 feet. Although there is loss in energy, the average velocity downstream of the sluice gate increases, which is compensated by a decrease in flow depth. For each flow rate, the average increase in velocity of the flow is approximately 0.064 feet per second. By adding the sluice gate and straightener, a minimal head loss was achieved while both increasing the flow velocity, as well as producing a more uniform velocity profile across the width of the flume.

5. Conclusions/Future Work

In summary, the full flume velocity profile was crucial in understanding how the flow through the flume behaved without any components or inserts in place. It is important to know all capabilities of equipment before making any changes or upgrades to a system. After realizing that both the tilting capabilities and varying flow rate were not enough to reach appropriate velocities, new steps were taken to design and create components to aid in creating new baselines for the flume. These steps included researching different ways to increase flow velocity while taking into account how they would work with the existing components already in the flume.

Next, by designing and creating a nozzle insert to work in conjunction with the sediment insert, the water velocity in the flume was doubled, while maintaining the ability to have both components placed in the flume. More importantly, the design of the

contraction was created to allow for future work to be done more easily, namely the ease of clearance by the 3D positioning device for the ADV probe and the clear test section walls for Particle Imaging Velocimetry (PIV) systems to be used.

Additionally, in order to understand the effects of scour and erosion on the substrate, a device for measuring displacement along with the methods necessary to determine the amount of sediment displaced were defined. The HR Wallingford bed profiler gives two-dimensional plots of the substrate to characterize the contours of the bed after being exposed to flow across the surface. As far as future work, a permanent fixture for the track and profiler will be designed and created to allow for accurate placement of the device across the width of the flume to be able to calculate volumes of displaced sediment more easily. With the addition of the fixture, more accurate methods to calculate displaced sediment must be developed.

Lastly, with the addition of the sluice gate and straightener, the increase in flow velocity and minimal head losses justifies the use of these flow control devices in the flume. By understanding how these devices affect the flow, energy data and velocity profiles will be considered as cylinders are placed in the test section, and later in the project model MHK devices, in such arrays that will be created in the river environments in which they will be placed. The creation of this testing platform with associated measurement methods will aid in the advancement of hydrokinetic device technologies and help predict the environmental effect on the local substrate more easily, so that eventually green energy can be added to our power grid more quickly.

6. References

[1] Beninati, M.L., Volpe, M.A., Riley D.R. and M.H. Krane, "Development of a Testing Platform for Scaled-Laboratory Studies of Marine Hydrokinetic Devices," Proceedings of American Geophysical Union – Ocean Sciences, San Francisco, CA, December 13-17, 2010.

[2] Çengel, Yunus A., and Cimbala, John M. *Fluid Mechanics: Fundamentals and Applications 2nd Edition.* New York: McGraw-Hill, 2010. Print.

[3] Doolan, Con J. "Numerical Evaluation of Contemporary Low-Speed Wind Tunnel Contraction Designs." The Journal of Fluids Engineering: Technical Brief. 2007.

[4] Garcia, C.M., Cantero, M.I., Nino, Y., and Garcia, M.H., 2005, "Turbulence Measurements with Acoustic Doppler Velocimeters" Journal of Hydraulic Engineering, 131(12), pp. 1062-1073.

[5] Hogarty, Dave. "East River Turbines Face Upstream Battle." *Gothamist*. 13 Aug. 2007. Web. 1 September 2010

[6] Howes, Daniel J., Burt, Charles M., Sanders, Brett F. "Subcritical Contraction for Improved Open-Channel Flow Measurement Accuracy with an Upward-Looking ADVM." Journal of Irrigation and Drainage Engineering ASCE. September 2010.

[7] Ida, Mizuho, Nakamura, Hideo, Nakamura, Hiroo, Takeuchi, Hiroshi. "Designs of Contraction Nozzle and Concave Back-Wall for IFMIF Target." Fusion Engineering and Design. 2004.

[8] Kraus, N.C., Lohrmann, A., and Cabrera, R., 1994 "New Acoustic Meter for Measuring 3D Laboratory Flows" Journal of Hydraulic Engineering, 120(3), pp. 406-412.

[9] Lang, Chris. "Harnessing Tidal Energy Takes New Turn." IEEE Spectrum Sept. 2003: 13.

[10] Marine Renewable Energy Research and Development Act of 2007.

[11] Martin, V., Fisher, T.S.R., Millar, R.G., Quick, M.C. 2002 "ADV Data Analysis for Turbulent Flows: Low Correlation Problem" Proceedings of Hydraulic Measurements and Experimental Methods Conference.

[12] McLelland, S.J. and Nicholas, A.P., 2000, "A new method for evaluating errors in High-frequency ADV measurements" Hydrological Processes, 14, pp. 351-366

[13] Sontek. Sontek *ADVField Acoustic Doppler Velocimeter Technical Documentation*.

[14] Voulgaris, G. and Trowbridge, J.H., 1998 "Evaluation of the Acoustic Doppler Velocimeter (ADV) for Turbulence Measurements" Journal of Atmospheric and Oceanic Technology, 15, pp. 272-289.

[15] Walmsley, Alan. "The Design, Construction, and Commissioning of the University of Otago Swimming Flume." ISBS - Conference Proceedings Archive, 17 International Symposium on Biomechanics in Sports (1999).

[16] Watmuff, Jonathan H. "Wind Tunnel Contraction Design." Proceedings of 9th Australasian Fluid Mechanics Conference, 8-12 December 1986.

[17] Wetzel, J.M., Arndt, R.E.A. "Hydrodynamic Design Considerations for Hydroacoustic Facilities: Part I – Flow Quality." St. Anthony Falls Hydraulic Laboratory Technical Paper 374 PTI – Series A. Volume 116, June 1994.

Appendix I

MATLAB Energy Curve Code (Created by Drew Riley)

```matlab
% Clean everything out
clear all
close all

% Input variables
Q1 = input('What is the first flowrate? (ft^3/s) ');
b1 = input('What is the width of the channel? (ft) ');
Q2 = input('What is the second flowrate? (ft^3/s) ');
Y1 = input('What is the water height upstream? (ft) ');
Y2 = input('What is the water height downstream? (ft) ');
g = 32.2;
y = linspace(.01,5,1000);
q1 = Q1/b1;
q2 = Q2/b1;

% Calculating Energy Head curve
for j = 1:1000
    E1(j) = y(j) + Q1^2/(2*g*(b1*y(j))^2);
end
% Calculating Energy Head curve
for k = 1:1000
    E2(k) = y(k) + Q2^2/(2*g*(b1*y(k))^2);
end
% Solving for actual Energy Head
Energy1 = Y1 + Q1^2/(2*g*(b1*Y1)^2)
Energy2 = Y2 + Q2^2/(2*g*(b1*Y2)^2)
Yc1 = (q1/g)^(1/3)
Yc2 = (q2/g)^(1/3)
% Yc and Ec
Emin1 = min(E1);
Emin2 = min(E2);


% Line for ansyntope for y axis
% E1 = linspace(1,5,1000);
% y1 = linspace(1,5,1000);

plot(E1,y,E2,y,'--')
axis([0 1.2 0 1.2])
xlabel('Energy (ft)')
ylabel('Water Height (ft)')
title('Energy Head Curve')
% text(Energy,Y,'\leftarrow Energy Head')
% text(Emin,Yc,'\leftarrow Critical Depth')
```